2012

Plasmon Enhanced Fluorescence (PEF) of High and Low Quantum Yield Molecules

Haider Mohan
University of Windsor

Plasmon Enhanced Fluorescence (PEF) of High and Low Quantum Yield Molecules

By

Haider Mohan

A Thesis

Submitted to the Faculty of Graduate Studies

Through Chemistry and Biochemistry

In Partial Fulfillment of the requirements for

the Degree of Master of Science

at The University of Windsor

Windsor, Ontario, Canada

2012

Plasmon Enhanced Fluorescence (PEF) of High and Low Quantum Yield Molecules

by

Haider Mohan

APPROVED BY:

I. Samson
Earth and Environmental Sciences

T. Carmichael
Department of Chemistry and Biochemistry

R. Aroca, Advisor
Department of Chemistry and Biochemistry

S. Ananvoranich, Chair of Defence
Department of Chemistry and Biochemistry

January 18, 2013

DECLARATION OF CO-AUTHORSHIP / PREVIOUS PUBLICATION

I. Co-Authorship Declaration

I hereby declare that this thesis incorporates material that is result of joint research, as follows:

This thesis incorporates the outcome of a joint research undertaken in collaboration with Ariel Guerrero, Pablo Albella under the supervision of Professor Ricardo Aroca. The collaboration is covered in parts of section 4.3 of Chapter 4 of the thesis. In all cases, the key ideas, primary contributions, experimental designs, data analysis and interpretation, were performed by the author, and the contribution of co-authors was primarily through the provision of theoretical calculations for the electric field of Au-SHIN, and synthesis and experiment execution of Au-SHIN rods.

I am aware of the University of Windsor Senate Policy on Authorship and I certify that I have properly acknowledged the contribution of other researchers to my thesis, and have obtained written permission from each of the co-author(s) to include the above material(s) in my thesis.

I certify that, with the above qualification, this thesis, and the research to which it refers, is the product of my own work.

II. Declaration of Previous Publication

This thesis includes [one] original paper that has been previously published in peer reviewed journals, as follows:

Thesis Chapter	Publication title/full citation	Publication status
Chapter 4	Aroca, R.F., et al., Plasmon-Enhanced Fluorescence and Spectral Modification in SHINEF. The Journal of Physical Chemistry C, 2011. **115**(42): p. 20419-20424.	Published

I certify that I have obtained a written permission from the copyright owner(s) to include the above published material(s) in my thesis. I certify that the above material describes work completed during my registration as graduate student at the University of Windsor.

I declare that, to the best of my knowledge, my thesis does not infringe upon anyone's copyright nor violate any proprietary rights and that any ideas, techniques, quotations, or any other material from the work of other people included in my thesis, published or otherwise, are fully acknowledged in accordance with the standard referencing practices. Furthermore, to the extent that I have included copyrighted material that surpasses the bounds of fair dealing within the meaning of the Canada Copyright Act, I certify that I have obtained a written permission from the copyright owner(s) to include such material(s) in my thesis.

I declare that this is a true copy of my thesis, including any final revisions, as approved by my thesis committee and the Graduate Studies office, and that this thesis has not been submitted for a higher degree to any other University or Institution.

ABSTRACT

A new branch of fluorescence has emerged with the use of metallic nanostructures to enhance optical signals: Plasmon enhanced fluorescence (PEF). In the literature it has grown with two different names: surface enhanced fluorescence (SEF) and also metal enhanced fluorescence (MEF).

In this thesis, we have explored some of the peculiar properties of plasmon enhanced fluorescence. In particular, we try to relate intrinsic molecular properties of fluorescence such as cross section and quantum yield to the enhanced signal. The source and basic properties of localized surface plasmon resonances is also discussed. The attention is then centre in the plasmon signature on the fluorescence spectrum or spectral profile modification. The matching of plasmon scattering and fluorescence emission assists in constructing fluorophore-nanoparticle systems for PEF applications. Specific experiments are discussed design to test the impact of the fluorophore quantum yield in observed enhancement. Finally, a practical technique to deliver the enhancing nanoparticles onto surfaces containing the analyte is also presented. The latter is intended for practical application and to ensure higher average enhancement values.

For my parents, my wife and my daughter

ACKNOWLEDGEMENTS

I would like to take this opportunity to thank many people who made accomplishing this goal a reality.

I start with my dear supervisor, Dr. Ricardo Aroca; it was possible to finish my graduate degree because of his knowledge and his support, scientifically and financially. It is his thirst and strive for scientific research that inspired me throughout my time here. I will always hold dear the coffee discussions that we had, where we discussed all aspects of life. You were a teacher in many ways.

I would also like to thank my committee members for giving me some of their valuable time in reading my work; Dr. Iain Samson, Dr. Tricia Breen Carmichael, and Dr. Sirinart Ananvoranich.

Thanks to the Department of Chemistry and Biochemistry for their financial support, and many thanks to Marlene Bezaire for her tremendous help and support. I would like to thank the whole MSSG family: Golam, Ariel, Aisha, Flavinho, Diogo, Gabriel, Kate, Pedro, Elena, Rosa, Rosana, Teo, Igor, and many more. I have learned a lot from them and truly enjoyed my time with them.

Perhaps, I cannot thank enough my parents: Adel and Wafaa, who sacrificed their life, work, and left their birth country to ensure a better life for me here in our beloved Canada. I hope one day I could show them that their effort was much appreciated.

Many thanks to my sister: Lubna and brothers Mustafa, and Mazin and his family, for their endless and appreciated support.

To my wife, Huda, I say thank you. You, and my baby girl (Joud) were my motivation to work hard, and I hope you will always be by my side in all our future endeavors.

TABLE OF CONTENTS

DECLARATION OF CO-AUTHORSHIP / PREVIOUS PUBLICATION.....iv

ABSTRACT.....vi

DEDICATIONS vii

ACKNOWLEDGEMENTS viii

LIST OF TABLES xiii

LIST OF FIGURES xiv

LIST OF ABBREVIATIONS xvii

CHAPTER 1 1

INTRODUCTION.....1

1.1 Introduction 2

1.2 References 4

CHAPTER 2 7

BACKGROUND 7

2.1 Introduction 8

2.2 Fluorescence Parameters 9

2.3 Plasmon Enhanced Spectroscopy.....11

2.4 Mechanism of Enhancement in Plasmon Enhanced Fluorescence 16

2.5 SHIN and SHINEF.....19

2.6 References 22

CHAPTER 3 26

INSTRUMENTATION AND SYNTHESIS 26

3.1 Introduction: 27

3.2 Thin Film Fabrication and Synthesis 27

3.2.1 Langmuir-Blodgett Deposition System 27

3.2.2 Synthetic Procedure for Colloidal Gold and Silver, and Shell-Isolated Nanoparticles. 30

3.2.2.1 Gold Colloids and SHIN 30

3.2.2.2 Silver Colloids and SHIN 32

3.3 Morphological Characterization 33

3.3.1 Scanning Electron Microscopy (SEM) 33

3.3.2 Transmission Electron Microscopy (TEM) 36

3.3.3 Atomic Force Microscopy (AFM) 37

3.4 Spectroscopic Characterization 39

3.4.1 UV-Vis Spectroscopy 39

3.4.2 InVia Renishaw micro-Raman System. 39

3.5 References 41

CHAPTER 4 43

SPECTRAL PROFILE MODIFICATION IN PLASMON ENHANCED FLUORESCNCE (PEF) 43

4.1 Introduction 44

4.2 Molecular Emission and NP Scattering Overlap 44

4.2 Experimental 46

4.3 Results and Discussion 48

4.4 Conclusion 53

4.5 References 54

CHAPTER 5 56

AVERAGE SHINEF AND SHINERS OF HIGH AND LOW QUANTUM YIELD MOLECULES 56

5.1 Introduction 57

5.2 Molecular Emission and Its Properties 58

5.3 Plasmon Enhanced Fluorescence Enhancement Channels 60

5.4 Experimental 62

5.5 Results and Discussion 63

5.5.1 Comparison of SHINERS and SHINEF of the Same Molecule. 63

5.5.2 Fluorescence-plasmon Overlap 72

5.5.3 Enhanced Emission from LB Monolayers 76

5.6 Conclusion 78

5.7 References 79

CHAPTER 6 82

A METHOD FOR APPLYING SHIN PARTICLES 82

6.1 Introduction 83

6.2 Hot Spot 83

6.3 Experimental 85

6.4 Results and Discussion 87

6.4.1 Ag-SHIN Characterization 87

6.4.2 UV-Vis of Spray Samples 90

6.4.3 SEM of Spray Samples. 91

6.4.4 EF Histogram of Spray Samples 95

6.5 Conclusion 97

6.6 References 98

CHAPTER 7 100

CONCLUSIONS 100

7.1 Conclusions 101

7.2 Future Work 103

VITA AUCTORIS 104

LIST OF TABLES

Table 2.1 Approximate values of cross cection for molecular processes. 9

Table 2.2 Terms of mathematical relation of electromagnetic radiation and dielectric particle.....13

Table 3.1: Properties of objective lenses used in InVia micro-Raman system.....41

LIST OF FIGURES

Figure 2.1 Jablonski diagram. 8

Figure 2.2 A dielectric particle in a harmonically oscillating electric field 12

Figure 2.3 Mie absorption and scattering components for silver nanoparticles. 16

Figure 2.4 Enhanced fluorescence profile as a function of fluorophore-NP separation. ... 18

Figure 2.5 Local electric field simulations and relative scattering cross sections done on Ag-SHIN particles with different shell thicknesses. 20

Figure 2.6 Theoretical simulations for the extinction cross section of SHIN with different sizes, shell thicknesses, and aggregation patterns 21

Figure 2.7 SEM images of SHIN particles applied as smart dust. 22

Figure 3.1 Langmuir film formation and Langmuir-Blodgett film deposition. 28

Figure 3.2 Surface pressure-molecular area LB isotherm 29

Figure 3.3 Scanning electron microscope. 34

Figure 3.4 SEM images obtained with BSE and SE detectors 35

Figure 3.5 SEM substrates used in SHIN characterization. 36

Figure 3.6 TEM instrument 37

Figure 3.7 Schematic presentation of atomic force microscopy used in Veeco Digital AFM microscope. 38

Figure 3.8 Carry 50 UV-Vis spectrometer 39

Figure 3.9 In Via Reinshaw micro-Raman system. 40

Figure 4.1 Plasmon absorption spectrum of Au-SHIN rods and spheres. 48

Figure 4.2 SEM and TEM image of Au-SHIN spheres and Au-SHIN rods. 49

Figure 4.3 PTCD fluorescence spectra for solution and LB monolayer. 50

Figure 4.4 Spectral profile modification in PTCD mixed monolayer using SHIN spheres and SHIN rods.....51
Figure 4.5 Mapping results for SHINEF of PTCD LB monolayer using Au-SHIN spheres 52
Figure 4.6 Mapping of Au-SHIN rods SHINEF on PTCD mixed LB monolayer 53
Figure 5.1 Plasmon absorption spectrum of sodium citrate reduced Ag-SHIN, crystal violet, and ethyl violet.....64
Figure 5.2 SEM images of Ag colloids and SHIN.....64
Figure 5.3 TEM images of Ag-SHIN.....65
Figure 5.4 SHINERS and SHINEF of ethyl violet with Ag-SHIN.....65
Figure 5.5 SHINERS and SHINEF of crystal violet with Ag-SHIN. 67
Figure 5.6 SEM and TEM images Ag-SHIN (reduced with hydroxyl amine). 68
Figure 5.7 SHINEF and SHINERS of crystal violet and ethyl violet using Ag-SHIN (reduced using hydroxyl amine) 69
Figure 5.8 Theoretical calculations for the enhanced local electric field of an Au-SHIN. 70
Figure 5.9 absorption spectra of Au-SHINs and ethyl violet.....71
Figure 5.10 SHINEF and SHINERS of ethyl violet solution using Au-SHINs (citrate reduction method). 71
Figure 5.11 Malachite green absorption and emission and Ag-SHIN (citrate reduction method). 73
Figure 5.11 SHINEF and SHINERS of malachite green using Ag-SHIN with 633 nm laser. 74
Figure 5.12 Enhancement results for malachite green and Ag-SHIN using the 514 nm excitation source. 75

Figure 5.13 SHINEF of chromeo 642 and R18 with Ag-SHIN. 77

Figure 6.1 SHIN drop cast under a light microscope. 84

Figure 6.2 Ag SHIN absorption spectrum imposed over R18 mixed LB emission spectrum. 87

Figure 6.3 SEM images of Ag colloids and SHIN 88

Figure 6.4 AFM images of Ag-SHIN. 89

Figure 6.5 Graphical representation of SHIN. 90

Figure 6.6 Absorption spectrum of the sprayed film. 91

Figure 6.7 SEM images of all SHIN spray samples with 2 µm scale bar. 92

Figure 6.8 SEM images of spray samples with 5 µm scale bar. 93

Figure 6.9 SEM images of all SHIN spray samples with 10 µm scale bar. 94

Figure 6.10 An overview of the SHIN spray samples. 95

Figure 6.11 (a-d) Enhancement factor (EF) histogram for the spray samples (5,10,15,20). 96

Figure 6.11 (e,f) The histogram of EF for 25, and 30 spray samples. 96

Figure 6.11 (g) EF distribution for a casted drop 97

LIST OF ABBREVIATIONS

AA	Arachidic Acid
AFM	Atomic Force Microscopy
APTMS	3-aminopropyltrimethoxysilane
BSE	Back Scattering Electrons
CCD	Charged Coupled Device
EF	Enhancement Factor
EM	Electromagnetic
HFW	Horizontal Field Width
LB	Langmuir-Blodgett
LL	Laser Line
LSPR	Localized Surface Plasmon Resonance
MEF	Metal Enhanced Fluorescence
NA	Numerical Aperture
NP	Nanoparticle
PEF	Plasmon Enhanced Fluorescence
PTCD	Perylene Tetracarboxylic Derivatives
R18	Octadecyl rhodamine B chloride
RRS	Resonance Raman Scattering
RS	Raman Scattering
SE	Secondary Electron
SES	Surface Enhanced Spectroscopy

SEF	Surface-enhanced Fluorescence
SEM	Scanning Electron Microscopy
SHIN	Shell Isolated Nanoparticle
SHINEF	Shell Isolated Nanoparticles-Enhanced Fluorescence
SHINERS	Shell Isolated Nanoparticles-Enhanced Raman Spectroscopy
SMD	Single Molecule Detection
SPR	Surface Plasmon Resonance
TEM	Transmission Electron Microscopy
UV-Vis	Ultraviolet-Visible

CHAPTER 1

INTRODUCTION

1.1 Introduction

Molecular fluorescence spectroscopy is emission between a singlet excited electronic state and the singlet ground electronic state. It is a common physical phenomenon with a wide range of applications [1-3]. Fluorescence is a powerful tool in biochemistry, biophysics, forensic science and biotechnology. Therefore, improvements in the technique are strongly encouraged and pursued. Improvements and new developments in terms of the technique sensitivity, the range of fluorophores, their stability, and the versatility of the experimental set ups are some of goals and motivators that helps move this particular scientific research forward. A new avenue of the scientific research is based on the use of noble metallic nanoparticles for fluorescence enhancement.

The idea of enhancing optical processes using noble metals was discovered for Raman scattering. It was first reported in 1977[4, 5]. Few years later the concept expanded to fluorescence[6] . Very early reports put forth detailed justification on the sources of enhancement of optical signals, pointing to the electromagnetic field enhancement in the surroundings of noble metal nanoparticles. The origin of the enhancement is in the plasmon excitation of the nanostructures. The technique names evolved since the emergence of the technique. Surface enhanced fluorescence or SEF term is widely used and the name carries the same notion found in Surface enhanced Raman scattering or SERS, as the technique happens on the surface of the metal nanostructuress. Metal enhanced fluorescence or MEF is also used denoting the fact that it is metals that enhance the fluorescence emission[7]. Plasmon enhanced fluorescence or PEF[8-10] is recently used, the name notes to the fact that it is the plasmon in the metallic nanoparticles that is responsible for the enhancements, and metals that support LSPR waves are capable of

producing intense enhanced fluorescence emission, with high enhancement factors and high sensitivity reaching single molecule regimes reproducibly[11, 12]. This thesis is titled Plasmon enhanced fluorescence of high and low quantum yield molecules. We chose the designation of fluorescence enhancement as plasmon produced phenomena, based on the experimental evidences showing the role of plasmonics, where they all point to the plasmon as the basis of optically enhanced processes.

Throughout our presented work we will see that the plasmon leaves a vivid mark on the enhanced fluorescence, Chapter 2 of the thesis will cover the basic elements of PEF starting with the fluorescence phenomenon itself, and transitioning to the origin of the plasmon and how the enhancement resulting from localized surface plasmon resonance (LSPR) is understood within the dipolar model, and the efficiency of the nanoparticle scattering. Mechanism of enhancement in PEF will also be discussed, and we will introduce the nanoparticle system we employ throughout the thesis, which is shell-isolated nanoparticle (SHIN).

Chapter 3 will discuss the main instrumentation used for the present work. Langmuir-Blodgett (LB) monolayer films will be reviewed as they are used to fabricate highly ordered 2D arrays of target molecules, with known and constant number of molecules per surface area. The synthesis routes used to make SHIN particles will also be described. Instruments used for surface and morphological characterization will also be discussed. These include scanning electron microscopy (SEM), transmission electron microscopy (TEM), and atomic force microscopy (AFM). Spectroscopic characterization of the nanoparticles and the analyte is described which includes UV-Vis, Raman and fluorescence spectroscopy.

In chapter 4, the changes in the spectral profile of the fluorescence spectrum are discussed. Plasmon contribution in PEF exceeds a mere increase in the fluorescence intensity to altering the resulting fluorescence profile, along with selectively enhancing regions of the emission spectrum. These changes further confirm the contribution of plasmon enhancement, which is an electromagnetic process happening irrespective of the presence of any analyte. Therefore it would be expected to contribute equally to molecules unrelatedly of their intrinsic quantum yield. The latter will be the focus of chapter 5 titled SHINEF and SHINERS of low and high quantum yield molecules.

In chapter 6, a practical and easy method for SHIN particles deposition will be introduced. The goal will be to create relatively more homogenous areas with higher than average enhancement via plasmon coupling (hot spots) of SHIN particles.

Chapter 7 contains the conclusions and some areas for future research.

1.2 References

1. Zimmer, M., *Green Fluorescent Protein (GFP): Applications, Structure, and Related Photophysical Behavior.* Chem. Rev. (Washington, D. C.), 2002. **102**(Copyright (C) 2012 American Chemical Society (ACS). All Rights Reserved.): p. 759-781.
2. Berezin, M.Y. and S. Achilefu, *Fluorescence Lifetime Measurements and Biological Imaging.* Chem. Rev. (Washington, DC, U. S.), 2010. **110**(Copyright (C) 2012 American Chemical Society (ACS). All Rights Reserved.): p. 2641-2684.

3. Germain, M.E. and M.J. Knapp, *Optical explosives detection: from color changes to fluorescence turn-on.* Chemical Society Reviews, 2009. **38**(Copyright (C) 2012 American Chemical Society (ACS). All Rights Reserved.): p. 2543-2555.

4. Albrecht, M.G. and J.A. Creighton, *Anomalously intense Raman-spectra of pyridine at a silver electrode.* Journal of the American Chemical Society, 1977. **99**(15): p. 5215-5217.

5. Jeanmaire, D.L. and R.P. Van Duyne, *Surface Raman spectroelectrochemistry. Part I. Heterocyclic, aromatic, and aliphatic amines adsorbed on the anodized silver electrode.* Journal of Electroanalytical Chemistry and Interfacial Electrochemistry, 1977. **84**(1): p. 1-20.

6. Wokaun, A., et al., *Energy transfer in surface enhanced luminescence.* Journal of Chemical Physics, 1983. **79**(1): p. 509-14.

7. Geddes, C.D. and J.R. Lakowicz, *Metal-Enhanced Fluorescence.* Journal of Fluorescence, 2002. **12**(2): p. 121-129.

8. Tam, F., et al., *Plasmonic enhancement of molecular fluorescence.* Nano Lett., 2007. **7**(2): p. 496-501.

9. Aroca, R.F., et al., *Plasmon-Enhanced Fluorescence and Spectral Modification in SHINEF.* The Journal of Physical Chemistry C, 2011. **115**(42): p. 20419-20424.

10. Moula, G. and R.F. Aroca, *Plasmon-Enhanced Resonance Raman Scattering and Fluorescence in Langmuir-Blodgett Monolayers.* Anal. Chem. (Washington, DC, U. S.), 2011. **83**(Copyright (C) 2012 American Chemical Society (ACS). All Rights Reserved.): p. 284-288.

11. Zhang, W., et al., *Giant and uniform fluorescence enhancement over large areas using plasmonic nanodots in 3D resonant cavity nanoantenna by nanoimprinting.*

Nanotechnology, 2012. **23**(Copyright (C) 2012 American Chemical Society (ACS). All Rights Reserved.): p. 225301/1-225301/9.

12. Fu, Y., J. Zhang, and J.R. Lakowicz, *Large enhancement of single molecule fluorescence by coupling to hollow silver nanoshells.* Chemical Communications, 2012. **48**(78): p. 9726-9728.

CHAPTER 2

BACKGROUND

2.1 Introduction

Molecules at room temperature occupy mainly the lowest vibration state v_o of the ground electronic state S_o, and in accordance with the Boltzmann factor. When irradiated with appropriate energy, molecules can absorb photons and occupy any of the quantum states; vibrational or electronic. An electronic absorption phenomenon occurs on the femto second scale (10^{-15} seconds). Rapidly after being excited, the molecule may undergo an internal or external relaxation within pico seconds (10^{-12}) and relax to the lowest vibronic state of the first excited singlet electronic state S_1. From that point, the excited molecule can undergo one of many paths of de-excitation. If there is radiative emission (photon emission) or fluorescence, the molecule returns to any of the vibrational states of S_0. In such scenario, the fluorescence profile will be red shifted with respect to the absorption profile (i.e. emitted photon is of lower energy or longer wavelength).

Figure 2.1 is a form of Jablonski diagram which depicts molecular electronic transitions as it interacts with electromagnetic radiation.

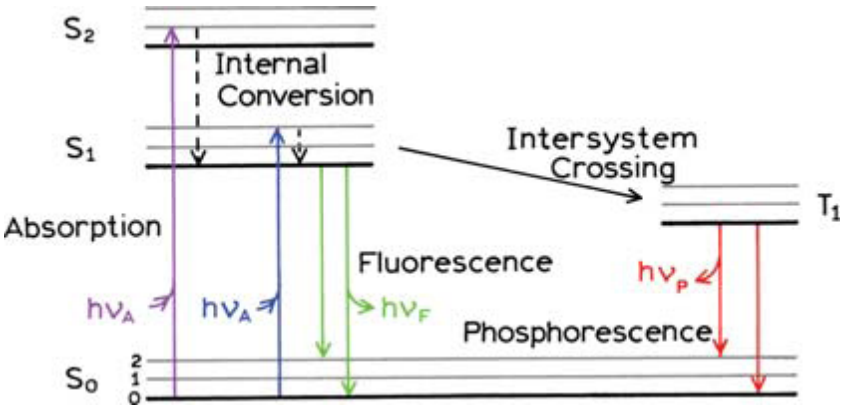

Figure 2.1 Jablonski diagram. Adapted from Joseph R. Lakowicz. Principles of Fluorescence Spectroscopy. 3rd Ed.

2.2 Fluorescence Parameters

Fluorescence may be considered an efficient process with large cross section relative to scattering. Fluorescence cross section is the probability of a molecule to emit light expressed as a sectional area per molecule, commonly in $cm^2 / molecule$. It is as large as absorption cross sections with the experimental advantage of emission detection. This makes fluorescence phenomena advantageous in detection techniques, due to the high sensitivity. Some typical values for common spectroscopic processes and molecular phenomena are shown in table 2.1

Process	Cross section (cm^2)
Fluorescence	10^{-19}
Rayleigh scattering	10^{-26}
Raman scattering	10^{-29}
Resonance Raman scattering	10^{-24}
SERRS	10^{-17}
SERS	10^{-19}
Absorption (Ultra Violet)	10^{-18}
Absorption (Infrared)	10^{-20}

Table 2.1 Approximate values of cross section for molecular processes.

It can be seen that fluorescence cross section is on par with highly enhanced techniques like surface enhanced Raman spectroscopy (SERS) and surface enhanced resonance

Raman scattering (SERRS). The fluorescence phenomenon finds many applications in medicine, biology, chemistry, physics and engineering. Considering the high cross section value for fluorescence, trace detection and single molecule detection are readily achieved.

Fluorescence efficiency is characterized by its quantum yield (*Q*), which is the ratio of emitted photons to the absorbed photons:

$$Q(\lambda) = \frac{number\ of\ \ photons\ emitted}{number\ of\ \ photons\ absorbed} \tag{2.1}$$

A molecule with high quantum yield would be highly efficient as it emits a large percentage of the photons it absorbs. Quantum yield could also be expressed in terms of excited state decay rates. Decay rate is the rate at which the excited molecule comes down to the ground state. Radiative decay describes molecular de-excitation processes accompanied by photon emission. The radiative decay rate Γ_r would be the inverse of the radiative life time. The latter is the intrinsic lifetime of the fluorophore

$$\tau_0 = \frac{1}{\Gamma_r} \tag{2.2}$$

Molecules in the excited electronic states can also relax by nonradiative processes where excitation energy is not converted into photons but are dissipated by thermal processes such as vibrational relaxation or collisional quenching. Γ_r *and* Γ_{nr} are the radiative and nonradiative decay rates respectively, and the quantum yield of the molecule is:

$$Q_0 = \frac{\Gamma_r}{\Gamma_r + \Gamma_{nr}} \tag{2.3}$$

The temporal evolution of the excited state can be described by

$$\tau = \frac{1}{\Gamma_r + \Gamma_{nr}} \tag{2.4}$$

The fluorescence lifetime, τ , of the fluorophore, measures the combined rate of the radiative and nonradiative pathways, that is the time the molecule stays in the excited state before it loses the excitation energy. The total decay rate is therefore the sum of both radiative and non-radiative decay rates, and it is the inverse of measured lifetimes. Therefore, we can also write the quantum yield as:

$$Q_0 = \frac{\Gamma_r}{\Gamma_r + \Gamma_{nr}} = \frac{\tau}{\tau_0} \tag{2.5}$$

2.3 Plasmon Enhanced Spectroscopy

The origin of the enhancement is in the plasmon excitation of the nanostructures. As the light of certain wavelength is irradiated on metallic nanostructure structures much smaller than the wavelength, the electric field in the light can excite the conduction electrons to oscillate coherently at the same frequency. These surface charges when oscillating resonantly (Fröhlich condition, discussed below) with the external field, they create a dipole that is capable of radiation (scattering). The collective oscillations are termed surface plasmon resonance. Mie in his work solved the Maxwell's equation for the extinction spectra (absorption and scattering) for a monochromatic plane interaction with a spherical particle[1].

The interaction of an electromagnetic field and spherical dielectric particles could be understood using the quasi-static approximation, with the assumption that the particle size is much smaller than the applied EM field wavelength. With this premise, one can assume that the phase of a harmonically oscillating field is constant over the particle volume. We will adopt the detailed representation outlined in Maier's book and the references mentioned therein.[2-4]

Figure 2.2 illustrates a representation of spherical dielectric particle in an oscillating electric field.

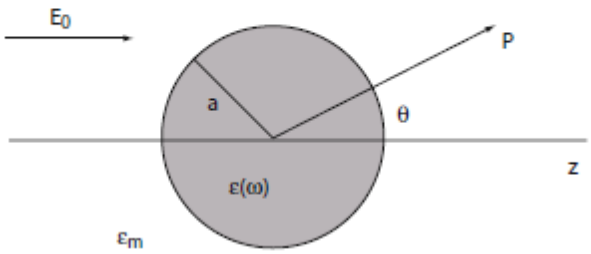

Figure 2.2 A dielectric particle in a harmonically oscillating electric field. Adapted from Maier, S.A., *Plasmonics: Fundamentals and Applications*2007, New York: Springer

The theory leads to a solution of the potential inside the particle to be:

$$\Phi_{in} = -\frac{3\varepsilon_m}{\varepsilon+2\varepsilon_m} E_0 r\, cos\theta \tag{2.6}$$

And the potential outside the particle:

$$\Phi_{out} = -E_0 r\, cos\theta + \frac{\varepsilon-\varepsilon_m}{\varepsilon+2\varepsilon_m} E_0 a^3 \frac{cos\theta}{r^2} \tag{2.7}$$

The terms in the equations presented here are displayed in table 2.2

Term	Physical quantity	Term	Physical quantity
Φ_{in}	Electric potential inside the dielectric sphere	a	Radius of the sphere
Φ_{out}	Potential outside the sphere	p	Dipole moment of the particle
E_0	Incident electric field	α	Polarizability of the particle
ε	Dielectric constant of the spherical particle, that is frequency dependant	C_{sca}	Scattering cross section of the particle
ε_m	Dielectric constant of the medium (e.g. 1 for vacuum)	C_{abs}	Absorption cross section of the particle
r	Distance outside the particle	k	$\frac{2\pi}{\lambda}$ λ is the wavelength of the oscillating field.

Table 2.2 Terms of mathematical relation of electromagnetic radiation and dielectric particle

It can be seen that the potential inside the sphere is in the opposite direction of the applied field. As for the potential outside the particle, the second term resembles that of an electric dipole

$$p = 4\pi\varepsilon_0\varepsilon_m a^3 \frac{\varepsilon-\varepsilon_m}{\varepsilon+2\varepsilon_m} E_0 \qquad (2.8)$$

While the complete solution provided by Mie theory accounts for multipole expansion, the dipole contribution is dominant in smaller sizes where the quasi-static assumption holds true. As the size increases the radiation damping effect leads to a reduction in the dielectric dipole.[5,6]

Using (p) in the equation (2.8), the external potential becomes

$$\Phi_{out} = -E_0 r\, cos\theta + \frac{p.r}{4\pi\varepsilon_0\varepsilon_m r^3} \quad (2.9)$$

Φ_{out} expression shows that the dipole is greatest when its vector located at $\theta = 0^{\circ}, 180^{\circ}$along the z direction of polarization. The magnitude of the dipole is proportional to the applied electric field, as well as the polarizability of the particle as seen in the following expression:

$$p = \varepsilon_0\varepsilon_m\alpha E_0 \quad (2.10)$$

Therefore the polarizability of a dielectric particle under a harmonically oscillating electric field with wavelength much larger than its volume is expressed as:

$$\alpha = 4\pi a^3 \frac{\varepsilon-\varepsilon_m}{\varepsilon+2\varepsilon_m} \quad (2.11)$$

The polarizability is a measurement of the particle response to external field, and it is apparent that the higher the polarizability, the higher the magnitude of the oscillating dipole and consequently the electric potential outside the particle. This notion is at the core of optically enhanced spectroscopies, since enhanced spectroscopy depends on the intensified potential in the near vicinity which presents itself in a form of an oscillating dipole.

The polarizability reaches a large value when the denominator approaches zero; such resonance condition happens when the real part of dielectric constant $\varepsilon(\omega)$of the metal is equal to $(-2\varepsilon_m)$, which is known as Fröhlich condition.

This condition is met in the visible range for few metallic nanoparticles, the most common ones used are Ag, Au, and Cu.

The general understanding of optical enhancement of fluorescence in terms of the cross sections will assist us in seeing the necessity of using noble metallic nanoparticles as enhancers.

The extinction cross section ($C_{ext} = C_{sca} + C_{abs}$), and its constitutents: absorption and scattering cross sections solution are shown below[4]:

$$C_{sca} = \frac{8\pi}{3} k^4 a^6 \left|\frac{\varepsilon - \varepsilon_m}{\varepsilon + 2\varepsilon_m}\right|^2 \quad (2.12)$$

$$C_{abs} = 4ka^3 Im\left[\frac{\varepsilon - \varepsilon_m}{\varepsilon + 2\varepsilon_m}\right] \quad (2.13)$$

The scattering cross section expression carries proportionality to$\left(\frac{1}{\lambda^4}\right)$ and (a^6), while the absorption cross section is proportional to$\left(\frac{1}{\lambda}\right)$ and (a^3) . This means that at smaller values of (a), C_{abs} will dominate. As the size of the nanoparticle increases, scattering efficiency will increase, and C_{sca} will dominate the extinction of the electric field by the particle.

Considering this fact, in addition to the need of particles much smaller than the wave length of the incident radiation, will help set minimum and maximum boundaries on optimal sizes for spherical nanoparticles for plasmon enhanced spectroscopy.

Figure 2.3 (left) illustrates the trend discussed above for the scattering and absorption cross section, in relation to the size of the nanoparticle. It can be seen that that for smaller NPs, the scattering cross section is much smaller than absorption cross section, while with

increasing size, the scattering cross section dominates over how the electric field interact with the nanoparticle. [7]

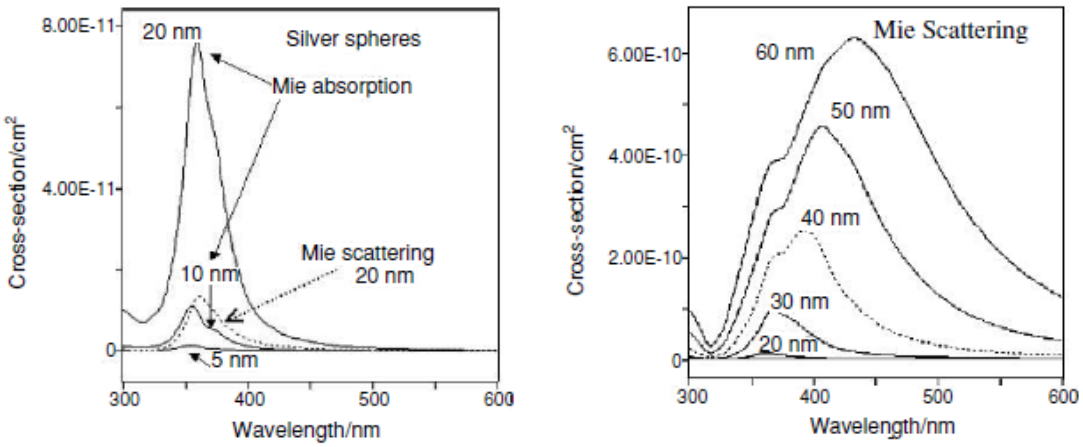

Figure 2.3 Mie absorption and scattering components for silver nanoparticles. Aroca, R., *Surface-enhanced Vibrational Spectroscopy*2006, Chichester: John Wiley & Sons**.**

As seen from Figure 2.3 (right), nanoparticles used for SES are good dipolar scatterers, with scattering cross section values reaching as high as 10^{-10} cm^2 which is seven orders of magnitude higher than the best fluorescence cross section ($10^{-17}cm^2$).

2.4 Mechanism of Enhancement in Plasmon Enhanced Fluorescence

In Surface enhanced Raman scattering, the process benefits from the close proximity to the enhancing nanostructure. The case in fluorescence is quite different.

In the immediate vicinity of the nanoparticle, the molecule -due to the intensified electric field- will see an enhancement in its absorption. The second effect the molecules feel from the nanoparticle is the creation of new pathways of energy de-excitation. One is the

reduction of radiative lifetime of the excited molecule, which will result in an increase in the radiative decay rate (see equation 2.2). The increase in the radiative decay rate will increase the modified quantum yield and thus the enhanced fluorescence

However, the nanoparticle could also provide nonradiative channels for de-excitation, via interaction with nanoparticle electron by Coulomb interaction. This will cause the dipole emitter to lose its excitation energy nonradiatively and the fluorescence will therefore be quenched.

The magnitude in the nonradiative decay rate is at its greatest on the particle surface, and vanishes at $(\frac{1}{d^3})$ where (d) is the distance from the NP surface[8].

The decay in the local field follows the expression$\left|\frac{a}{a+d}\right|^6$, where (d) is the distance from the NP surface and (a) is the radius of the NP. The profile of the enhanced fluorescence will emerge as a combination of these two processes. At short distance, the fluorescence will be quenched because the non radiative decay is very large and will dominate over the enhancement in radiative decay rate. But since the nonradiative enhancement decays faster than the local field, at a certain distance, fluorescence will still benefit from the near field average intensity enhancement$\langle|E|^2\rangle$ (to be discussed in a separate chapter), with no obscurity from the fluorescence quenching. This trend (shown in figure 2.4) [9] has been experimentally confirmed over the years many times by varying a spacer layer thickness between the enhancing NP and the fluorophore [10- 15]

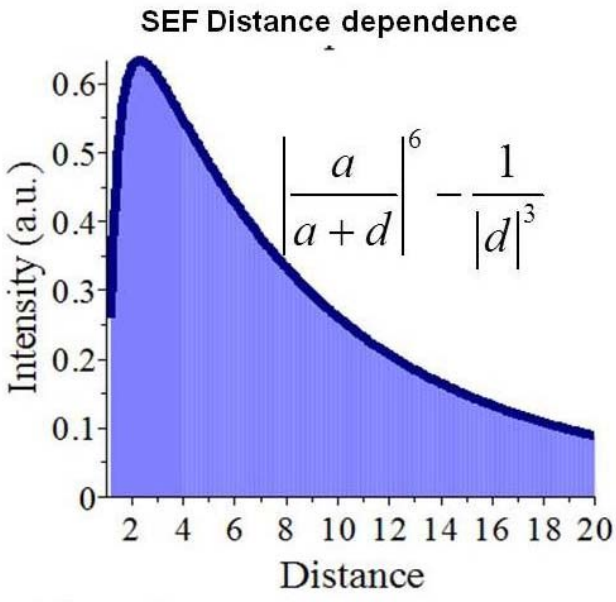

Figure 2.4 Enhanced fluorescence profile as a function of fluorophore-NP separation. Aroca, R.F., *Plasmon enhanced spectroscopy*. submitted, 2013

It can be seen now that SEF enhancement would not be able to benefit from the highest local field at the surface, due to that separation, since a separator between the NP and the chromophore is required. In practice, the spacer layer should be optimized to achieve maximum fluorescence.

If the molecular emission dipole resonates with same energy as the plasmon dipole, coupling between the two dipoles could occur; the nanoparticle -as a good scatterer- will emit the molecular emission to the far field where it could be detected.

Distinction between average SEF and single molecule (SM) SEF is important; the trend shown above where the fluorescence follows a clear distance dependence is for average SEF. In hotspot SEF the enhancement may be larger due to a coupling of local electric fields between neighbouring nanoparticles. Highly localized area between nanoparticles

provide high enhanced local field termed “hotspot” and have been shown to provide very high enhancement factors for fluorescence[16, 17]. Coupled field producing such large enhancement values are highly localized, e.g. in the case of dimer, the hot spot would be located in the vicinity between the two particles [18].

2.5 SHIN and SHINEF

All the preceding discussion regarding the surface enhanced fluorescence was setting parameters to what constitute a good SEF substrate.

The system we work with throughout the thesis is a class of nanoparticles named shell isolated nanoparticle (SHIN). They consist of a nanoparticle core of metals that supports localized surface plasmon resonance (LSPR), and coated with inert material like SiO_2 or Al_2O_3.

The synthetic development of SHIN particles span all the way back to coating materials with silica in what later was known as Stober method[19], a variation of the method was introduced by Liz-Marzan et al[20], for cases where the metal core is vitrophobic. Their application in SES was done for SERS and the technique was termed shell-isolated nanoparticle-enhanced Raman scattering (SHINERS)[21] and also for shell-isolated nanoparticle-enhanced fluorescence (SHINEF)[22]

The coating thickness could be well controlled, and tuned to put the fluorescence outside the quenching limits. The method proved to be successful in coating a variety of sizes and shapes in both gold and silver nanoparticles as we will see throughout the thesis. Theoretical calculations on models of SHIN show good values for the local electric field (see figure 2.5 left), the relative scattering cross section for Ag-SHIN with different shell

thicknesses is also plotted and shows an increase with in cross section with thinner shells (figure 2.5 right). Calculations show high cross section values (figure 2.6) for individual nanoparticles[23], the calculations also reveal a more intense local field values on aggregates of nanoparticles due to plasmon coupling, shown in same figure.

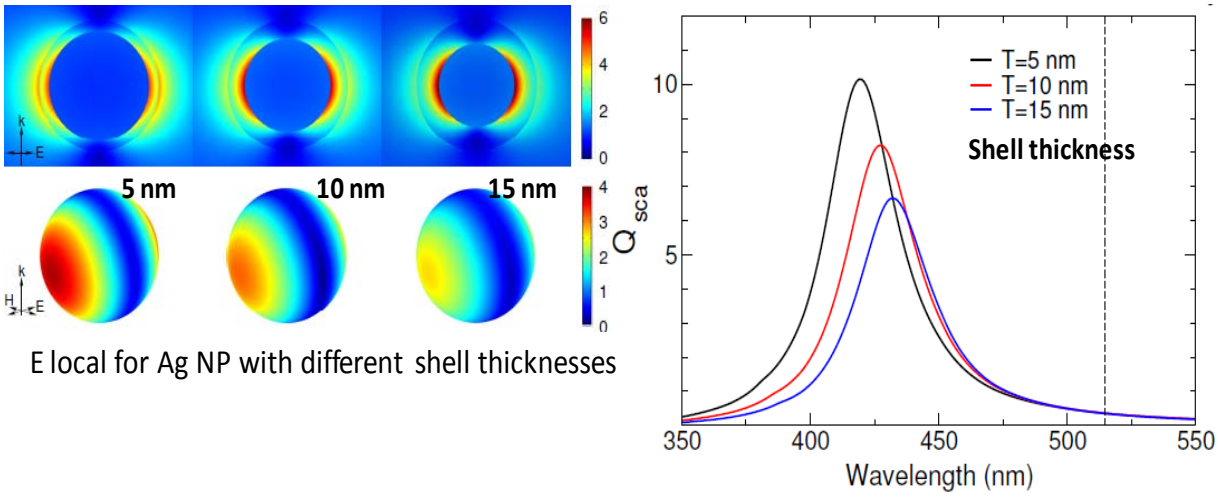

Figure 2.5 Local electric field simulations and relative scattering cross sections done on Ag-SHIN particles with different shell thicknesses. (Jose A Sanchez-Gil, Instituto de Estructura de la Materia,CSIC., private communication).

Figure 2.6 shows the calculation for the extinction cross section (absorption + scattering)in spherical SHIN particles, the simulation is done for several core sizes and several shell thicknesses, shown here the results of single, dimer, trimer aggregates.

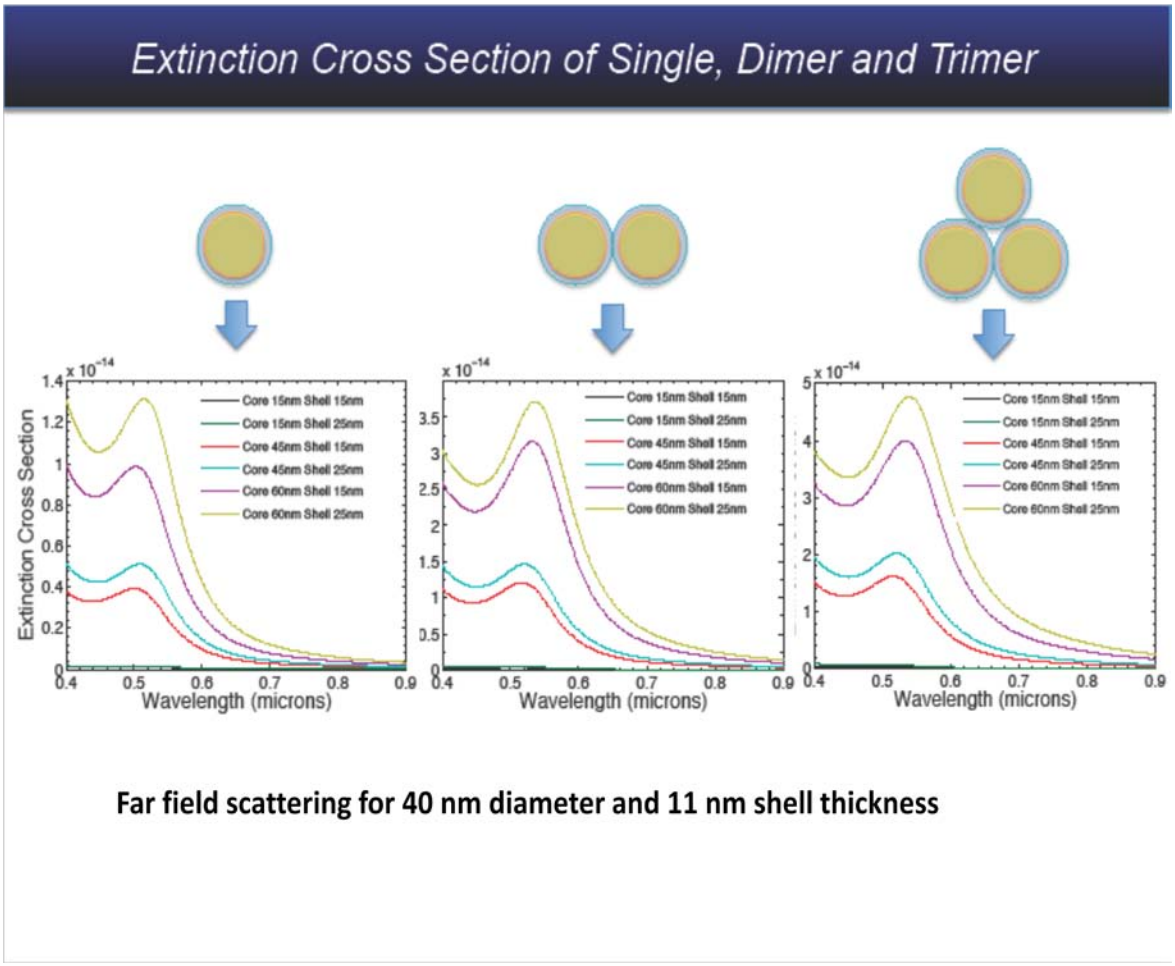

Figure 2.6 Theoretical simulations for the extinction cross section of SHIN with different sizes, shell thicknesses, and aggregation patterns. Adapted from Aroca, R.F., et al. 2011.

The SHIN substrate most important advantage is in its practicality. The SHIN particles could be used in many experimental setups regardless of the surface compositions and morphology. They could be applied simply as smart dust on the surface to be probed. Figure 2.7 shows SEM images of SHIN particles applied as smart dust, with different magnifications. SHIN core-shell design is shown on the bottom left inset of figure 2.7

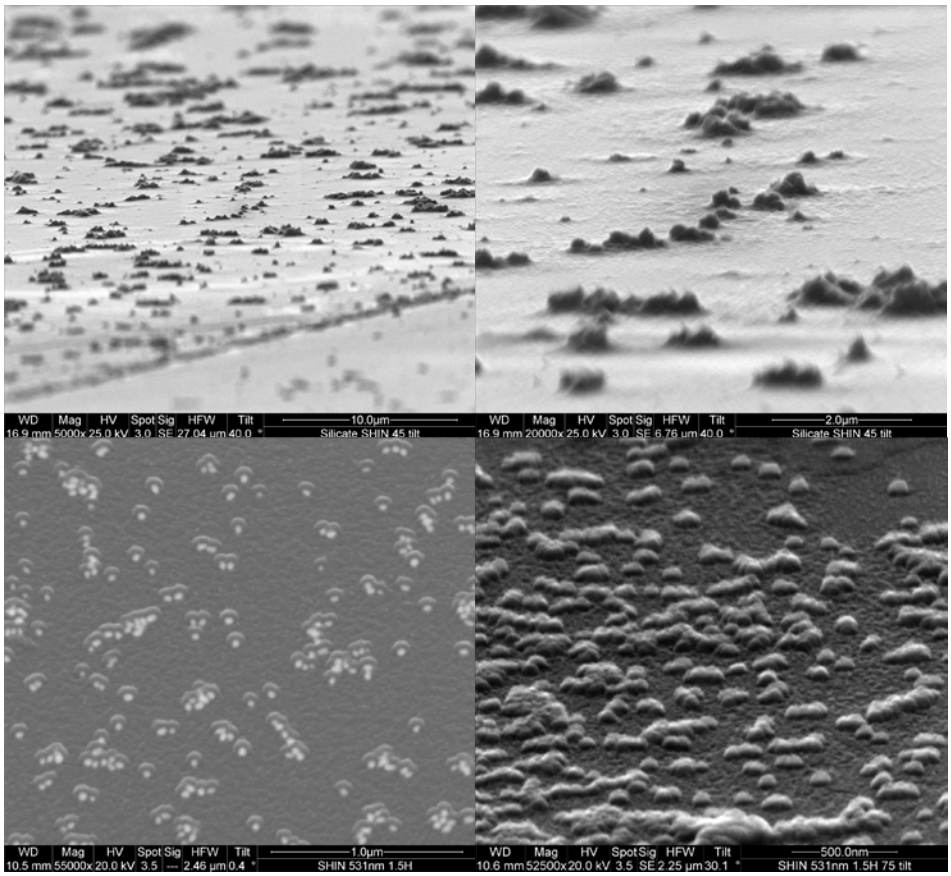

Figure 2.7 SEM images of SHIN particles applied as smart dust.

2.6 References

1. Mie, G., *Contributions to the Optics of Turbid Media, Especially Colloidal Metal Solutions.* Ann. Phys. (Weinheim, Ger.), 1908. **25**(Copyright (C) 2012 American Chemical Society (ACS). All Rights Reserved.): p. 377-445.
2. Maier, S.A., *Plasmonics: Fundamentals and Applications*2007, New York: Springer.
3. Jackson, J.D., *Classical Electrodynamics*. 3rd Edition ed1999, New York, NY: John Wiley&Sons, Inc.

4. Bohren, C.F., Huffman, Donald R., *Absorption and scattering of light by small particles*. First edition ed1983, New York, NY: John Wiley & Sons, Inc.

5. Meier, M. and A. Wokaun, *Enhanced fields on large metal particles: dynamic depolarization.* Opt. Lett., 1983. **8**(Copyright (C) 2012 American Chemical Society (ACS). All Rights Reserved.): p. 581-3.

6. Kokkinakis, T. and K. Alexopoulos, *Radiative decay of surface plasmons in small silver particles.* Phys. Rev. Lett., 1972. **28**(Copyright (C) 2012 American Chemical Society (ACS). All Rights Reserved.): p. 1632-4.

7. Aroca, R., *Surface-enhanced Vibrational Spectroscopy*2006, Chichester: John Wiley & Sons.

8. Gersten, J. and A. Nitzan, *Spectroscopic properties of molecules interacting with small dielectric particles.* Journal of Chemical Physics, 1981. **75**(3): p. 1139-1152.

9. Aroca, R.F., *Plasmon enhanced spectroscopy.* submitted, 2013.

10. Wokaun, A., et al., *Energy transfer in surface enhanced luminescence.* Journal of Chemical Physics, 1983. **79**(1): p. 509-14.

11. Aroca, R., et al., *Fluorescence enhancement from Langmuir-Blodgett monolayers on silver island films.* Langmuir, 1988. **4**(3): p. 518-21.

12. Anger, P., P. Bharadwaj, and L. Novotny, *Enhancement and Quenching of Single-Molecule Fluorescence.* Phys. Rev. Lett., 2006. **96**(11): p. 113002-1 to 113002-4.

13. Ray, K., R. Badugu, and J.R. Lakowicz, *Distance-dependent metal-enhanced fluorescence from Langmuir-Blodgett monolayers of alkyl-NBD derivatives on silver island films.* Langmuir, 2006. **22**(20): p. 8374-8378.

14. Bardhan, R., N.K. Grady, and N.J. Halas, *Nanoscale Control of Near-Infrared Fluorescence Enhancement Using Au Nanoshells.* Small, 2008. **4**(10): p. 1716-1722.

15. Akbay, N., J.R. Lakowicz, and K. Ray, *Distance-Dependent Metal-Enhanced Intrinsic Fluorescence of Proteins Using Polyelectrolyte Layer-by-Layer Assembly and Aluminum Nanoparticles.* Journal of Physical Chemistry C, 2012. **116**(19): p. 10766-10773.

16. Gill, R. and E.C. Le Ru, *Fluorescence enhancement at hot-spots: the case of Ag nanoparticle aggregates.* Physical Chemistry Chemical Physics, 2011. **13**(36): p. 16366-16372.

17. Zhang, W.H., et al., *Giant and uniform fluorescence enhancement over large areas using plasmonic nanodots in 3D resonant cavity nanoantenna by nanoimprinting.* Nanotechnology, 2012. **23**(22).

18. Cang, H., et al., *Probing the electromagnetic field of a 15-nanometre hotspot by single molecule imaging.* Nature, 2011. **469**(7330): p. 385-+.

19. Stober, W., A. Fink, and E. Bohn, *Controlled Growth of Monodisperse Silica Spheres in Micron Size Range.* Journal of Colloid and Interface Science, 1968. **26**(1): p. 62-&.

20. LizMarzan, L.M., M. Giersig, and P. Mulvaney, *Synthesis of nanosized gold-silica core-shell particles.* Langmuir, 1996. **12**(18): p. 4329-4335.

21. Li, J.F., et al., *Shell-isolated nanoparticle-enhanced Raman spectroscopy.* Nature, 2010. **464**(7287): p. 392-395.

22. Guerrero, A.R. and R.F. Aroca, *Surface-Enhanced Fluorescence with Shell-Isolated Nanoparticles (SHINEF).* Angew Chem Int Ed Engl, 2010(Copyright (C) 2012 U.S. National Library of Medicine.).

23. Aroca, R.F., et al., *Plasmon-Enhanced Fluorescence and Spectral Modification in SHINEF*. The Journal of Physical Chemistry C, 2011. **115**(42): p. 20419-20424.

CHAPTER 3

INSTRUMENTATION AND SYNTHESIS

3.1 Introduction:

1. **Thin Film Fabrication and Synthesis**
    i. **Langmuir-Blodgett Films**
    ii. **Synthetic Procedure for Colloidal Gold and Silver, and Shell-Isolated Nanoparticles.**
2. **Morphological Characterization**
    i. **Scanning Electron Microscopy (SEM)**
    ii. **Transmission Electron Microscopy (TEM)**
    iii. **Atomic Force Microscopy (AFM)**
3. **Spectroscopic Characterization**
    i. **UV-Visible Spectroscopy**
    ii. **Raman Scattering and Fluorescence Spectroscopy**

3.2 Thin Film Fabrication and Synthesis

3.2.1 Langmuir-Blodgett Deposition System

Langmuir-Blodgett deposition systems use is essential whenever there is a need for a highly controlled deposition of monomolecular layers on substrates. The need to control the spatial distribution of the analyte in a monolayer film is necessary to study the properties of plasmon enhanced spectroscopy. A general scheme of LB technique is depicted in figure 3.1

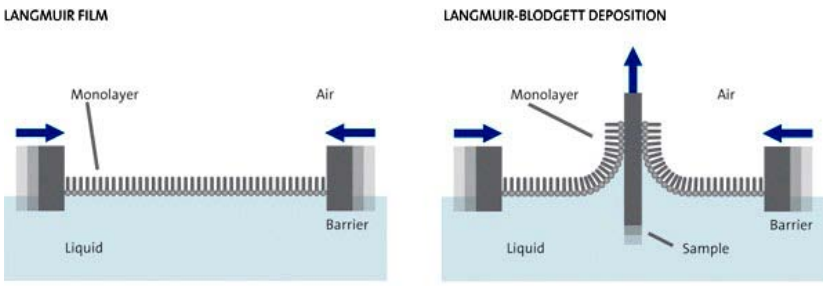

Figure 3.1 Langmuir film formation and Langmuir-Blodgett film deposition. Adapted from KSV NIMA

Using the Langmuir-Blodgett technique, it is possible to fabricate 2 dimensional nanometric films with thickness determined by the molecular size. The film is made from a solution of the target amphiphilic molecules in volatile organic solvents spread on air-aqueous interface. Aqueous subphase is ultra pure milli Q water (resistivity of 18.2 MΩ). The hydrophilic part of the molecules faces the aqueous side, while the hydrophobic side faces the air.[1]

The Nima Langmuir-Blodgett trough system is electronically controlled, with compressing barriers and a dipping device. After casting the solution, the solvent is left to evaporate for at least 30 minutes. As the trough starts compressing the films, the analyte molecules are far away from each other and could be thought of as molecules existing in a gaseous phase, with continuous compression, the inter molecular distance decreases gradually and the isotherm shows a gradual phase change from gaseous to liquid to ultimately solid phase. In the solid phase, there should be little or no separation between the molecules. For LB fabrication, the floating monolayer is compressed to a set surface pressure, then the dipping device lift a substrate that would have been immersed

prior to the casting step, keeping the film pressure constant, and transferring the floating monolayer to the substrate.[2]

Figure 3.2 depicts the different phases in the formation of mixed Langmuir films at different regions of the isotherm. The cartoon represents a mixed monolayer film of analyte and arachidic acid.

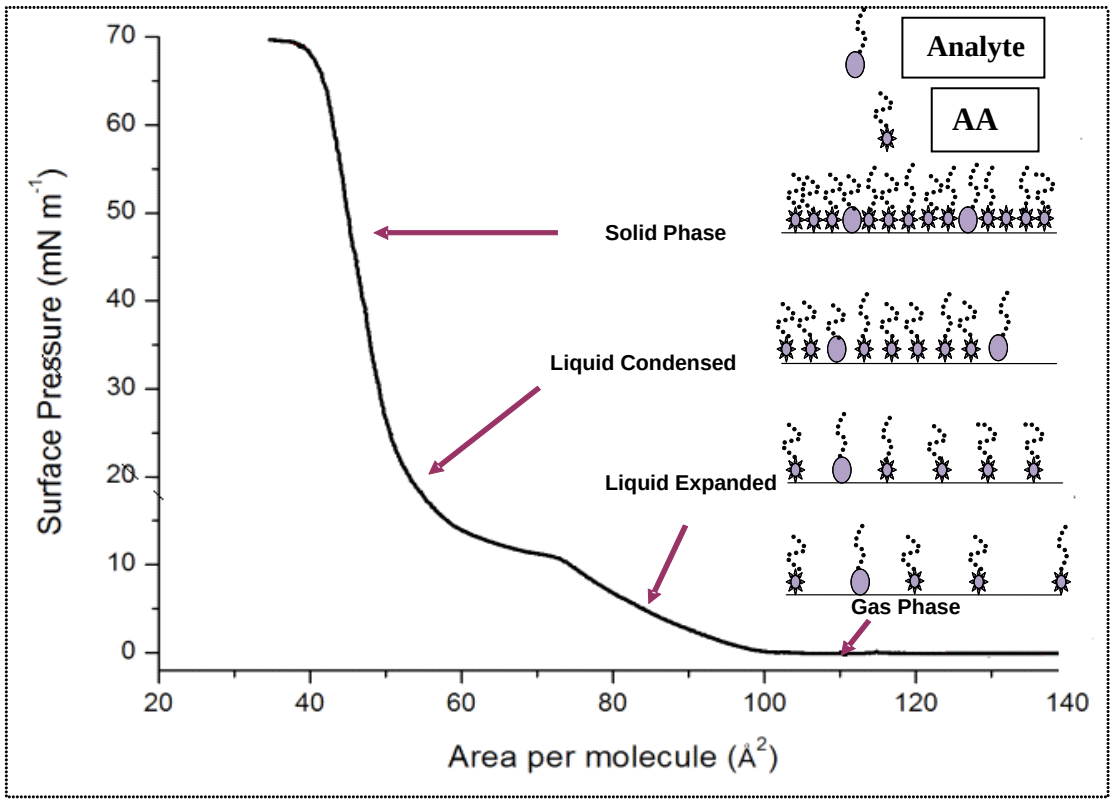

Figure 3.2 Surface Pressure-molecular area LB isotherm.

3.2.2 Synthetic Procedure for Colloidal Gold and Silver, and Shell-Isolated Nanoparticles.

There are two types of SHINs synthesized for SHINEF applications: Shell-Isolated gold Nanoparticles, and Shell-Isolated silver Nanoparticles.

For the synthesis of nanoparticles, the glassware used was cleaned with a freshly prepared aqua regia solution (1:3 HNO_3:HCl v/v) and washed with abundant amount of triply distilled milli Q water. milli Q water is used in all synthetic work, unless stated otherwise.Tetrachloroauric acid ($HAuCl_4.3H_2O$), citric acid trisodium salt (C6H5Na3O7), 3-amino propyl trimethoxysilane ($H_2N(CH_2)_3Si(OCH_3)_3$) (APTMS), sodium silicate, silver nitrate (AgNO3), tetraethylorthosilicate ($Si(OC_2H_5)_4$) (TEOS), hydroxyl amine (NH_2OH), were purchased from Sigma-Aldrich and used without further purification. Cation exchange resin (Amberlite IR-120, H^+ form; 16-45 mesh) was purchased from Fluka.

Gold colloids and subsequent silica coating were prepared following the method reported by Grabar et al, and Li et al, respectively with some modifications.[3,4]

3.2.2.1 Gold Colloids and SHIN

A 50 mL 0.01% HAuCl4 (w/v) was brought to boiling in a round bottom flask equipped to a condenser, with vigorous magnetic stirring in a sand bath. When the solution started to boil, 800 μl of 1% (w/v) trisodium citrate was added. A purplish red colour started to develop within 1 minute, heating and magnetic stirring was continued for another 10 minutes. The heat was then removed, but the stirring continued for 15 minutes. A small

amount of the resulting colloids were characterized with UV-Vis absorption and shows a surface plasmon absorption peak at 531 nm. Coating the gold NP was initiated by adding 3 mL of a freshly prepared solution of 1mM APTMS under vigorous magnetic stirring. Meanwhile, a 0.54 % (w/v) sodium silicate solution was prepared and activated by adjusting its pH down to 10.4 using the cation exchange resin to prompt the formation of silica.

The solution was heated again in a water bath to 90 °C, and then 9 mL of the active sodium silicate solution was added. Coating was continued for 1.5 hours. The resulting SHIN solution was concentrated by centrifugation at 12,000 rpm for 7 min and discarding the supernatant.

Au-SHINs used for the quantum yield experiment (see section 4.5.1) were synthesized as above with the following modification: A 150 mL solution of $HAuCl_4.3H_2O$ was made in milli Q water to a concentration of $5x10^{-4}$ M and heated to 80-90 °C in a round bottom flask in sand or water bath with vigorous magnetic stirring and under reflux, and the flask was covered with aluminum foil during the whole synthesis. Once the solution reached the mentioned temperature, 1.2 mL of 1mM sodium citrate was added to the gold solution. A slow change in colour was observed over a few minutes, heating the solution was continued to 30 minutes, then the flask was lifted from heat and stirring was continued for another 15 minutes.

The plasmon absorption maximum was recorded at 542 nm for the prepared colloids. The silica coating was the same as above and amounts were proportional to the present batch volume (9 mL of APTMS and 27 mL of activated silica solution added).

3.2.2.2 Silver Colloids and SHIN

Ag-SHINs were prepared via two different chemical routes, sodium citrate reduction and hydroxyl amine reduction. It should be noted that some of the batches prepared below were done with Yun Zhang's help based on the modifications she performed in her work.[5]

Sodium citrate reduction method was carried as described by Lee and Meisel.[6] 36 mg of $AgNO_3$ were dissolved in 200 mL water in a round bottom flask equipped to a condenser and heated in a sand bath to 190 °C, while vigorously stirred. When the solution started to boil, 4 mL of 1% (w/v) sodium tricitrate was added to the solution, boiling was continued for another hour. Solution was lifted from heat and absorption measurement was taken. Plasmon peak was very broad with a maximum at 413 nm. At this point, the pH of the colloids was adjusted to 10.5 using NaOH. While the solution was still warm, 12 mL of 1 mM APTMS was added and stirring was continued for another 15 minutes. The solution as heated again to 95 C in a water bath, 27 mL of active 0.54% (w/v) sodium silicate solution was added and coating process was carried for 3 hours. The resulting Ag-SHINs were then centrifuged at 11000 rpm for 7 minutes, and the supernatant was discarded. There were several batches consisting of 150 mL $AgNO_3$ starting solution, all other reagents were downscaled accordingly and proportionally.

The other method of reduction was reported by Leopold and Lendl[7] with some modification, by using hydroxyl amine as the reducing agent at a basic pH medium. 34 mL of 1.5×10^{-3} M hydroxylamine solution was added to a beaker and adjusting the pH to 10 using 1 M NaOH. Then, 1 mL of 1×10^{-2} M $AgNO_3$ solution was added drop wise,

while stirring for additional 25 minutes. Coating was done according the procedure reported by Wang et al with some modification.[8] 2 mL of the resulting silver nanoparticles solution were added into 6mL ethanol, and then pH was adjusted back to 10 with the same NaOH solution, after that 4µL of TEOS was added to the mixture. The mixture left standing in room temperature for 1 hour then Ag-SHINs particles were centrifuged at 11000 rpm for 7 minutes, and discard the supernatant.

3.3 Morphological Characterization

3.3.1 Scanning Electron Microscopy (SEM)

SEM was essential in determining several characteristics of SHIN particles. SEM uses a magnetically focused beam of electrons emitted by a tungsten emission gun. Since the wavelength of the electrons are much smaller than that of visible light; techniques like SEM and TEM could be used to probe surfaces with a much higher resolution than that accessible by light microscope. Resolution limits could go up to 5 nm in SEM, and 1 A in TEM used for characterization of SHIN in this work. The electrons in SEM hit the surface of the specimen and get reflected and/or scattered to a detector above the sample. Figure 3.3(A) illustrates how the SEM works, figure 3.3(B) shows a picture of the SEM microscope at Great Lakes Institute for Environmental Research (GLIER), which was employed in presented work

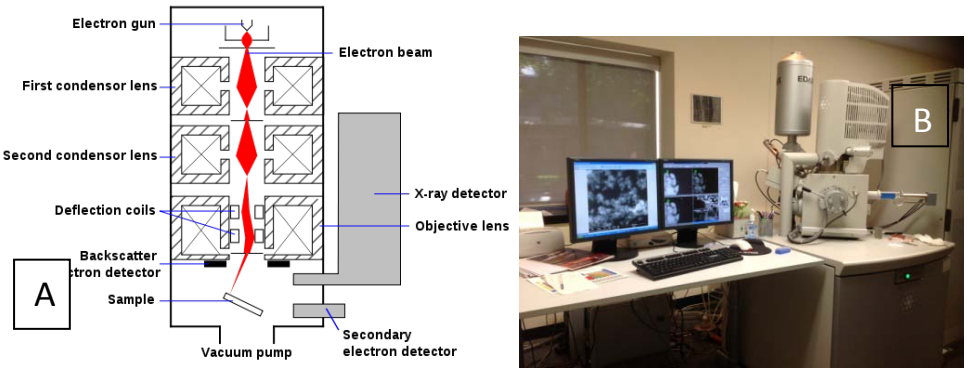

Figure 3.3 Scanning electron microscope. Figure (A) adapted from Wikimedia Commons, image in figure (B) is taken by author.

The scanning electron microscope used here is a FEI Quanta 200 FEG, with a field emission gun (filament), equipped with an Everhart-Thornley secondary electron detector, a solid state backscatter detector, and using (EDS) X-Ray detector for EDX (Energy-dispersive X-ray) analysis. The contrast degrees in the back scatter electron image (BSE) could be correlated to the heaviness of atoms, i.e. gold is heavier than carbon or silicon, and scatters more electrons, thus it appears to be brighter than either. While the secondary electron images (SE) contrast is a result of difference in surface morphology; higher surfaces appear to be brighter. An illustration is shown in Figure 3.4, where the left image is taken with BSE detector, while the image on the right is taken with SE detector.

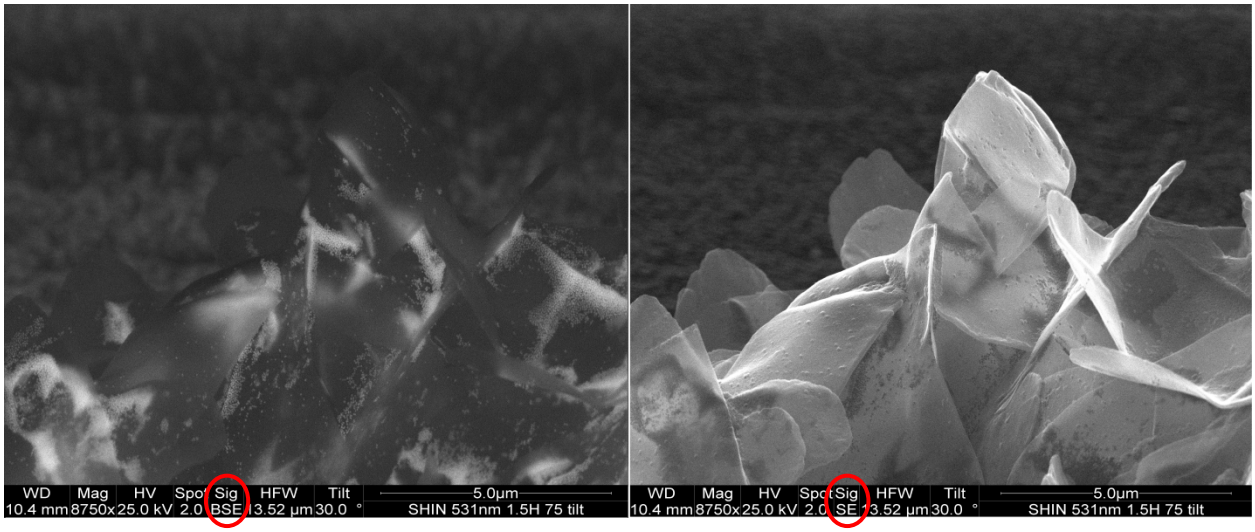

Figure 3.4 SEM images obtained with BSE and SE detectors

Utilizing both images enabled us to extract useful pieces of info; e.g. the size and shape distribution of SHIN, the quality and relative thickness of silica coating around NP, and last but not least the pattern for aggregation of SHIN.

Samples could be examined in top view and side view, by varying the angle at which the sample is located with respect to the electron beam and detectors. Some of the images presented throughout the thesis are of side view (figure 3.4). Because SEM works using electrons, conductive surfaces are required to prevent a build up of excess electrons on the probed surface, The substrates used here are: glass, MICA, Cu grids (typically used for TEM analysis as well), and HOPG (Highly Ordered Pyrolytic Graphite). Figure 3.5 shows SEM images of some of the substrates used for SHIN characterization. Left image is a side view of Cu grid with SHIN particles casted on top, inset is magnified image of the mesh. Center image is a top view of HOPG disc with SHIN particles casted on top. Right image is a carbon coated mica substrate showing the flat multi layered surface.

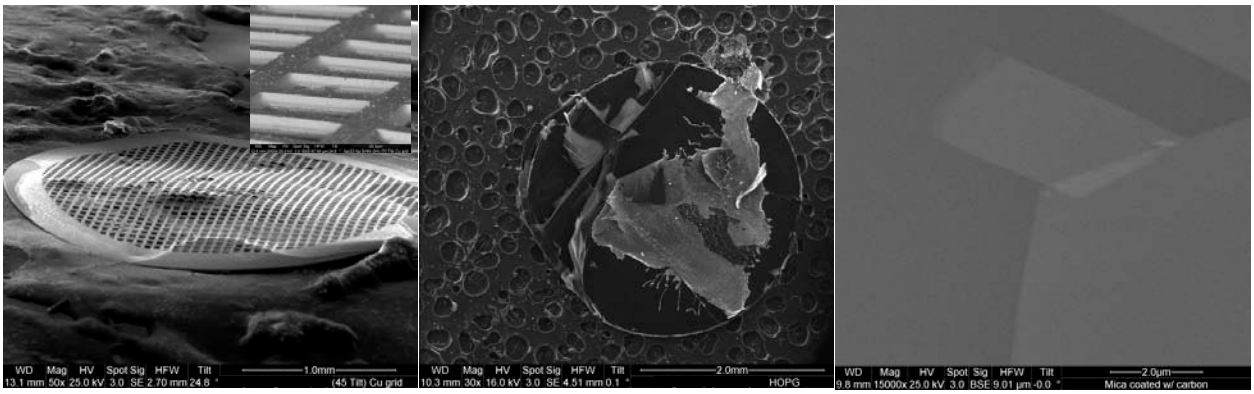

Figure 3.5 SEM substrates used in SHIN characterization.

In cases, where the substrate is not conductive, additional coating of conductive material is required, namely carbon coating. It is worth noting that this carbon coating would slightly reduce the resolution of images, much like details being obscured by covering them with a blanket. Presented SEM analysis took place at the Great Lakes Institute for Environmental Research (GLIER).

3.3.2 Transmission Electron Microscopy (TEM)

Like SEM, TEM uses a source of electron for illumination, but instead of probing the surface, the electrons pass through the samples were the detector are located behind the samples. This configuration allows the TEM to examine the cross sections of the material, and thus it is used to determine with high accuracy the silica shell thickness and the quality of the coating. Corresponding images in this thesis are obtained using the FEI Titan 80-300 Cubed TEM with a CEOS-designed hexapole-based aberration corrector and high-tension supply. Figure (3.6) represents the TEM used in the Canadian Center for Electron Microscopy where the TEM analysis took place.

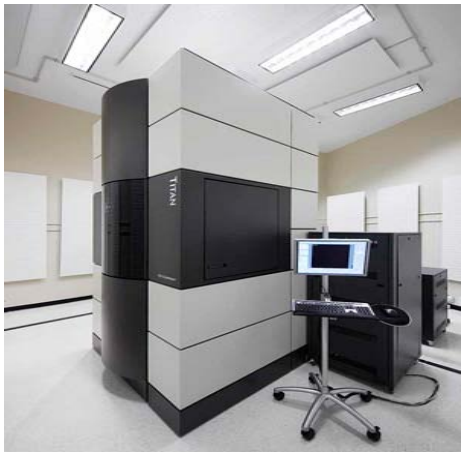

Figure 3.6 TEM instrument. Adapted from the Canadian Center for Electron Microscopy

3.3.3 Atomic Force Microscopy (AFM)

The third mean of visualizing surface morphology used here was AFM, unlike SEM and TEM, electrons are not used to probe the surface, rather, a very small tip (ca.12 nm) typically made of Si or Si_3N_4, scan over a sample, the tip is attached to a cantilever, and laser is illuminated on the back of the cantilever. Any change in the reflected laser is correlated to the deflection in the cantilever, tip and in turn the morphology among other properties of the surface. See figure 3.7(a) for AFM concept, figure 3.7(b) shows Veeco Digital AFM microscope

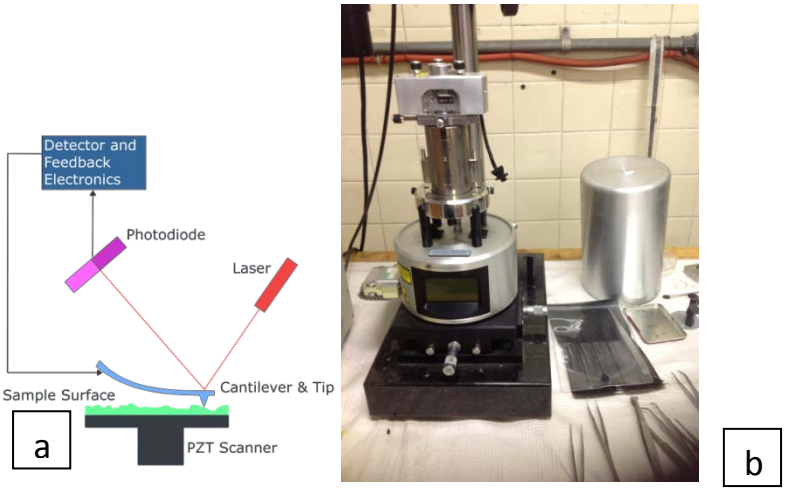

Figure 3.7 Schematic presentation of Atomic Force Microscopy used in Veeco Digital AFM microscope. Figure 3.7 (A) adapted from Wikimedia Commons. Image in figure 3.7 (B) is taken by author.

Since forces between the tip and surface can move the tip, there are different kinds of information that could be extracted: surface roughness, height of the surface, and softness of the surface. The scanning mode in the aforementioned system is either contact mode or tapping mode.

In tapping mode the cantilever oscillates near its natural resonance frequency with minimal taps to the surface, thus it is used in soft or easily damaged samples. As the cantilever scan over, if it hits high or low features, the amplitude of oscillation changes.[9] The frequency and phase of oscillation changes depending on other properties i.e. how hard or soft the surface is. Combining all the different channels of feedback different images are constructed that reveal the changes in amplitude of oscillation, the height of surface features, and to some extent different compositions in the surface.

In contact mode; the cantilever drags the tip across the surface, while being maintained at constant deflection, changes in surface features, surface friction will cause changes in the

deflection of the cantilever and imaged accordingly. The AFM images obtained here are done with tapping mode on fixated SHIN particles to minimize their movement across the surface of substrate. The AFM instrument used here is The Veeco Digital Instrument Multi Mode SPM with Nano IV control hardware. See Figure 3.7(b).

3.4 Spectroscopic Characterization

3.4.1 UV-Vis Spectroscopy

Molecular and plasmonic absorption for analyte and colloids respectively were obtained with a Cary 50 UV-Vis spectrometer. It is a single beam scan system with spectral range of 190-1100 nm. A picture of the machine is shown in figure (3.8).

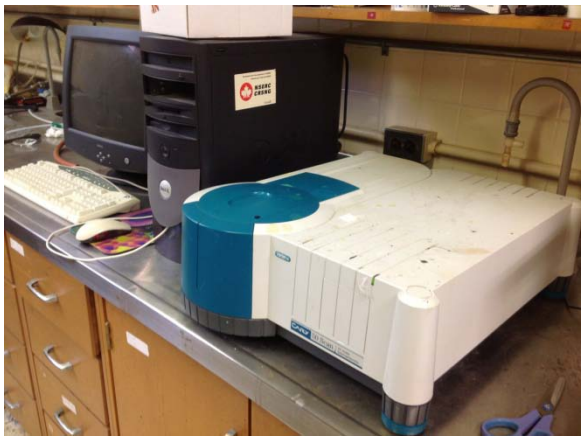

Figure 3.8 Carry 50 UV-Vis spectrometer. Image is taken by author.

3.4.2 InVia Renishaw micro-Raman System.

All Fluorescence, enhanced fluorescence, Raman scattering, enhanced Raman scattering measurements were carried out using the InVia system shown in figure (3.9). Image (A)

of the figure shows the laser lines used (L- R) 785nm, 632.8nm, 514nm. Figure 3.9 (B) shows the XYZ motorized stage equipped with a microscope.

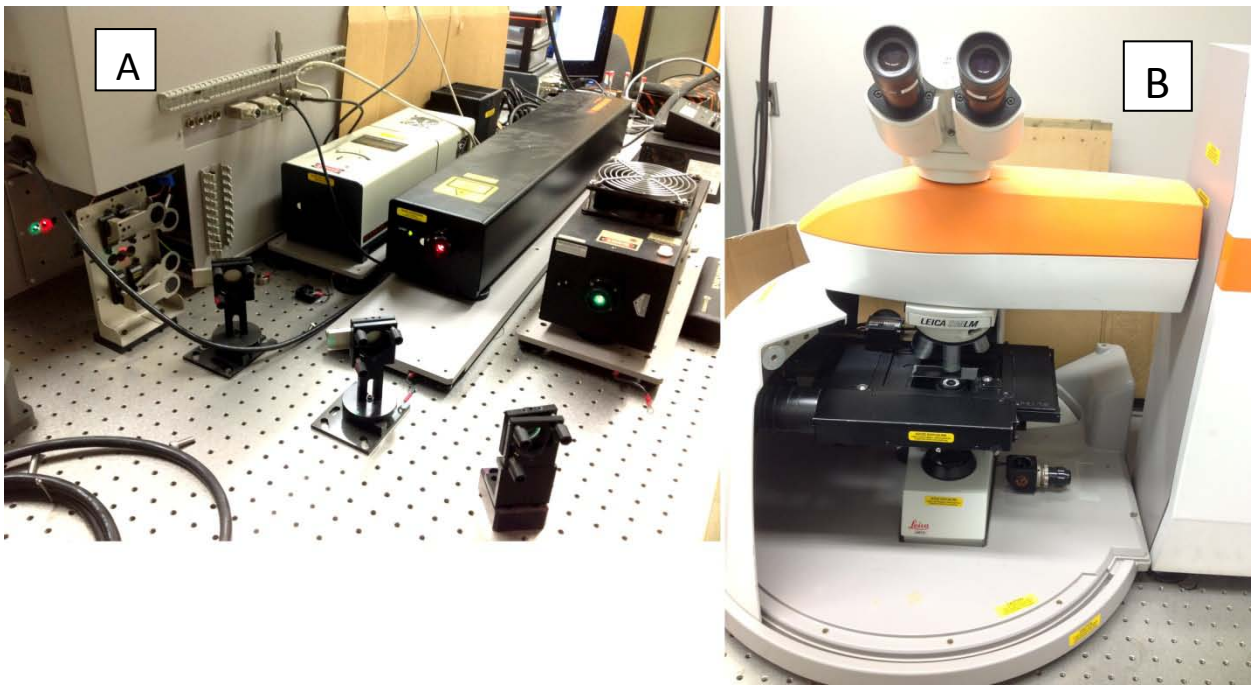

Figure 3.9 In Via Reinshaw micro-Raman system. Images are taken by author.

The micro-Raman system allows for high spatial resolution of measurements where the probed area and the excitation energy density is known and thus ultra sensitive detection could be readily achieved. The machine is equipped with several components that are of central importance to the work presented. These components will be discussed briefly. The InVia system spectrometer is manufactured by Renishaw (Reinshaw, UK), and is equipped with a cooled charged coupled device (CCD). The instrument is computer controlled with optics design that could accommodate different laser lines. The laser lines used in the instrument are 514.5 nm, 632.8nm, and 785nm. It is worthy to be noted here that the use of different excitation energies is crucial because different nano structures plasmon would be excited by different energies through the visible spectrum and also to

ensure various analyte systems could be excited by these different energies. The laser intensity could be controlled in the machine by a set of neutral density (ND) filters that could control the intensity of passing laser in preset values down to 0.00025%.

Another crucial component of the general experimental set up in SHINEF and SHINERS measurements is Raman-microscopy. High resolution collection is done by coupling the spectrometer to a microscope. With 180 degree collection geometry, both the excitation and collections are done via a set of magnification lenses that could focus the laser on a very small area (as small as 1 um^2). The system is equipped with several objective lenses that provide laser focusing to various areas as seen in table (3.1); the lenses differ in their Numerical Aperture (NA) value which determines the light collections efficiency.

Objective	NA	Spot Size, μm^2
5X	0.12	50
20X	0.40	20
50X	0.75	1
100X	0.90	< 1
f/15	0.34	30

Table 3.1: Properties of objective lenses used in InVia micro-Raman system

3.5 References

1. Roberts, G., *Langmuir-Blodgett Films*1990, New York: Plenum Press.
2. Dynarowicz-Latka, P., A. Dhanabalan, and O.N. Oliveira, *Modern physicochemical research on Langmuir monolayers.* Adv. Colloid Interface Sci., 2001. **91**(Copyright (C) 2012 American Chemical Society (ACS). All Rights Reserved.): p. 221-293.

3. Li, J.F., et al., *Shell-isolated nanoparticle-enhanced Raman spectroscopy.* Nature, 2010. **464**(7287): p. 392-395.

4. Grabar, K.C., et al., *Preparation and Characterization of Au Colloid Monolayers.* Analytical Chemistry, 1995. **67**(4): p. 735-743.

5. Guerrero, A.R., Y. Zhang, and R.F. Aroca, *Experimental Confirmation of Local Field Enhancement Determining Far-Field Measurements with Shell-Isolated Silver Nanoparticles.* Small, 2012. **8**(Copyright (C) 2012 American Chemical Society (ACS). All Rights Reserved.): p. 2964-2967.

6. Lee, P.C. and D. Meisel, *Adsorption and surface-enhanced Raman of dyes on silver and gold sols.* J. Phys. Chem., 1982. **86**(Copyright (C) 2012 American Chemical Society (ACS). All Rights Reserved.): p. 3391-5.

7. Leopold, N. and B. Lendl, *A New Method for Fast Preparation of Highly Surface-Enhanced Raman Scattering (SERS) Active Silver Colloids at Room Temperature by Reduction of Silver Nitrate with Hydroxylamine Hydrochloride.* J. Phys. Chem. B, 2003. **107**(Copyright (C) 2012 American Chemical Society (ACS). All Rights Reserved.): p. 5723-5727.

8. Wang, R., et al., *Preparation of Ag@SiO2 Dispersion in Different Solvents and Investigation of its Optical Properties.* J. Dispersion Sci. Technol., 2011. **32**(Copyright (C) 2012 American Chemical Society (ACS). All Rights Reserved.): p. 532-537.

9. Lombardi, J.R. and R.L. Birke, *A Unified View of Surface-Enhanced Raman Scattering.* Acc. Chem. Res., 2009. **42**(Copyright (C) 2012 American Chemical Society (ACS). All Rights Reserved.): p. 734-742.

CHAPTER 4

SPECTRAL PROFILE MODIFICATION IN PLASMON ENHANCED FLUORESCNCE (PEF)

4.1 Introduction

The introduction of plasmon enhanced fluorescence using shell-isolated nanoparticles provides many advantages and facilitates further investigation on the nature of plasmon-fluorophore interaction and its role in the enhanced emission process.

We saw throughout chapter 2 of this thesis, that several parameters in the nanoparticle are crucial in tuning the enhancement to maximize and diversify the applications of SEF. The question arises on how much the plasmon affect the molecular emission, and whether in addition to magnitude, there would be further modifications in the resulting fluorophore spectrum. The fluorophore interaction with plasmon is manifested in many forms. The plasmon will increase the intensity of the electric field in the immediate vicinity of the nanoparticle (near field) and thus increases the excitation rate for any neighboring fluorophore. The plasmon, at very short distances, modifies the lifetime of the excited states by providing additional channels of de-excitation, these channels could be radiative and thus increasing the radiative decay rate, or non-radiative and the excited molecules loses the excitation energy in a radiationless manner. First and foremost, there is also the coupling of the nanoparticle scattering to the molecular emission.

4.2 Molecular Emission and NP Scattering Overlap

The main component of the plasmon for nanoparticles of this size is the oscillating dipole.[1]

For nanoparticle of sizes (10 -100 nm), the scattering dipole is dominant and the scattering cross section is in the 10^{-12} cm^2 range, which is several orders of magnitude

larger that the fluorescence cross section. When there is an overlap between the plasmon oscillating dipole and the fluorophore emission dipole, the intensity of the emission in the far field - where it can be detected- increases.

Due to that frequency dependant, only emission frequencies coinciding with the dipole oscillation are intensified. This understanding helps further tune and improve the field of plasmon enhanced fluorescence.

This modification in the spectral profile of fluorophores will be following the profile of the enhancing nanoparticles [2, 3]. Research has come very far in terms of tailoring nanoparticles in many sizes, shapes and arrays. These advances open a window towards selective enhancement that could be done among several dyes, or even selectively enhancing certain emission pathways.

To examine the role of plasmon in modifying the emission spectral profile, well organized and ordered Langmuir-Blodgett monolayers of bis(3,4-dichlorobenzylimido) perylene (chloro-PTCD) mixtures with arachidic acid (*n*-eicosanoic acid)(1-10 respective ratio)are used. The PTCD molecule showcased here has bulky substituent groups on the chromophore, which favor planar **π**-stacking in high concentration [4]. The reference LB dye concentration is high and is ideal for aggregates that produce fluorescence spectrum characterized by the presence of both monomer and excimer emission. The excimer emission is a result of coupling of two or more molecules in the excited state and emitting as a couple. It is usually broad and does not have any structure[5].

Two nano structures are used; Au-SHIN spheres, and Au-SHIN rods. These two different nanostructures both support LSPR but in different regions of the visible spectrum and will interact with the PTCD emission differently.

4.2 Experimental

SHIN particle synthesis. Glassware used was cleaned with aqua regia (1:3 v/v ratio of nitric acid/ hydrochloric acid) and rinsed abundantly with ultrapure milli-Q water. The solvent used in all solutions preparation is ultrapure milli-Q water unless stated otherwise. Chemicals were purchased from Sigma Aldrich and used without any further purification unless otherwise stated. SHINs were prepared according to the method described by Grabar et al.[6] and Li et al.[7] with some modifications. The gold core was prepared by reducing tetrachloroauric acid (HAuCl4) with sodium citrate as outlined in section 3.2.2 in chapter 3.

Synthesis of nanorods was performed by Ariel Guerrero as follows: nanorods are synthesized adapting the method proposed originally by Nikobaakht and El-Sayed[8]. Tetrachloroauric acid ($HAuCl_4.3H_2O$), cetyltimethylammonium bromide (CTAB), sodium borohydride ($NaBH_4$), ascorbic acid and tetraethylorthosilicate (TEOS) were purchased from Sigma-Aldrich and used without further purification. A seed solution is prepared by adding, under constant stirring at 28°C, 50 µL of a 0.05 M $HAuCl_4$ solution into a flask containing 10 mL of a 0.100 M CTAB solution. To this solution we add 600 µL of a freshly-prepared ice-cold solution of $NaBH_4$ 10 mM. Upon addition of $NaBH_4$, the solution turns yellow-brownish. This solution was left undisturbed for a minute before

use. A growth solution is prepared, in parallel to the seeds, by adding consecutively and under constant stirring at 28°C, 10 mL of a 0.100 M CTAB solution, 100µL of a 0.004 M $AgNO_3$ solution, 100 µL of a 0.05 M $HAuCl_4$ solution, and 100 µL of 0.1 M ascorbic acid solution. The growth solution turns from yellow to colourless upon addition of ascorbic acid. After this was completed, 24 µL of the seeds solution were added to the growth solution, always stirring at 28°C. The solution started fading very slowly to blue, and the reaction is completed after about 30 minutes.

The silica coating of this solution was done following Gautier et al.[9]. The resulting nanorods solution was alkalinized by adding tiny droplets of a 1M NaOH solution until the pH reaches 10.5. At this point, three additions of TEOS 20%v/v in methanol were made with intervals of 30 minutes, adding 50 µL of TEOS every time. After the third addition, the solution was left to stand for 12 hours. After this, the solution was filtered through a Whatman No. 1 paper to remove the excess of CTAB, and concentrated by centrifugation at 12000 rpm, collecting the sediment. 3 µL of this concentrated solution was cast over the glass slide containing the mixed chloro-PTCD -arachidic acid LB film.

Plasmon characterization was done using a Cary 50 scan UV-Visible spectrometer. SEM characterization was carried out using a FEI quanta scanning electron microscope using a solid state backscatter detector and an Everhart-Thornley secondary electron detector. TEM images were obtained with a FEI Titan 80-300. Fluorescence measurements were performed using a micro-Raman Renishaw InVia system, with laser excitation at 514.5 and ca. 20 µW at the sample. Collection was done with a backscatter geometry using 20 X objective lens for focusing and probing area of 20 μm^2. 2D mapping with computer controlled (XYZ) encoded stage and a rastering step collection of 5 µm.

Langmuir monolayer of bis(3,4-dichlorobenzylimido) perylene (chloro-PTCD) and arachidic acid (*n*-eicosanoic acid) 1-10 mixtures was prepared at the air-water interface of a Nima film balance (model 302M).Langmuir film was made in the water-air interface by spreading a solution with dichloromethane as solvent. The Langmuir film was left for ca. 30 minutes to ensure a complete evaporation of the solvent. The film was then compressed by a couple of moving barriers at a speed of 5 cm^2/min, and constant pressure. The Langmuir film is deposited on pre cleaned corning 2048 microscope glass slide under constant pressure.

4.3 Results and Discussion

Figure 4.1 shows the plasmon absorption of Au-SHIN sphere with a maximum at 531 nm (4.1 B), and Au-SHIN rods with absorption maximum at 685 nm (4.1 A).

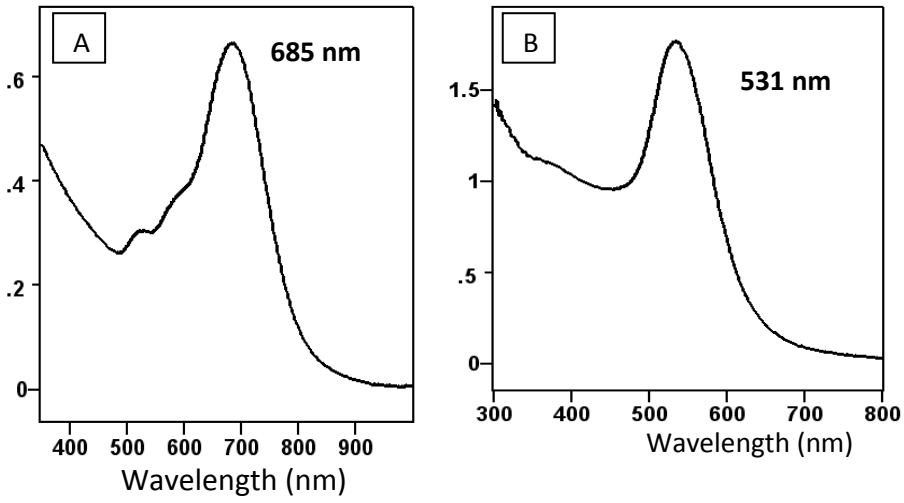

Figure 4.1 Plasmon absorption spectrum of (A) Au-SHIN rods and (B) spheres.

Both plasmon appear to have a narrow bandwidth, with the spheres having one maximum since the particles are round in shape, while the rods appears to have two maxima, the peak at 685 nm corresponds to plasmon oscillation in the longer side of the rod and the smaller shoulder around 550 corresponds to the shorter sides of the rod. Seeing the ratio of the intensity of two peaks, confirms that the rod yield in the colloids was adequate.

Figure 4.2 shows SEM and TEM images for spherical Au-SHINs (A,B), and TEM image of Au-SHIN rods (C). Both sets clearly shows the metallic core with a homogenous silicate shell around, in both techniques gold appears to be contrasted to the silica shell as they are different in heaviness and consequently the way they interact with the instrument stream of electrons.

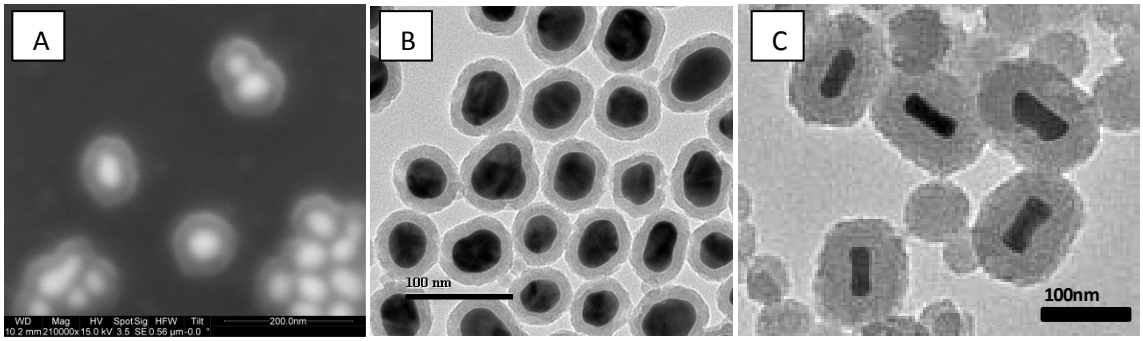

Figure 4.2 (A, B)SEM and TEM image of Au-SHIN spheres and (C) Au-SHIN rods.

From TEM images, shell thickness is estimated to be around 10 nm for the spheres, for the rods the silica shell appears to be thicker (40-50 nm)

Figure 4.3 shows the emission profile of the PTCD solution and PTCD mixed LB monolayer. Where the monomer peak is dominant in the solution spectrum, and the excimer emission is the most intense peak in the mixed LB emission.

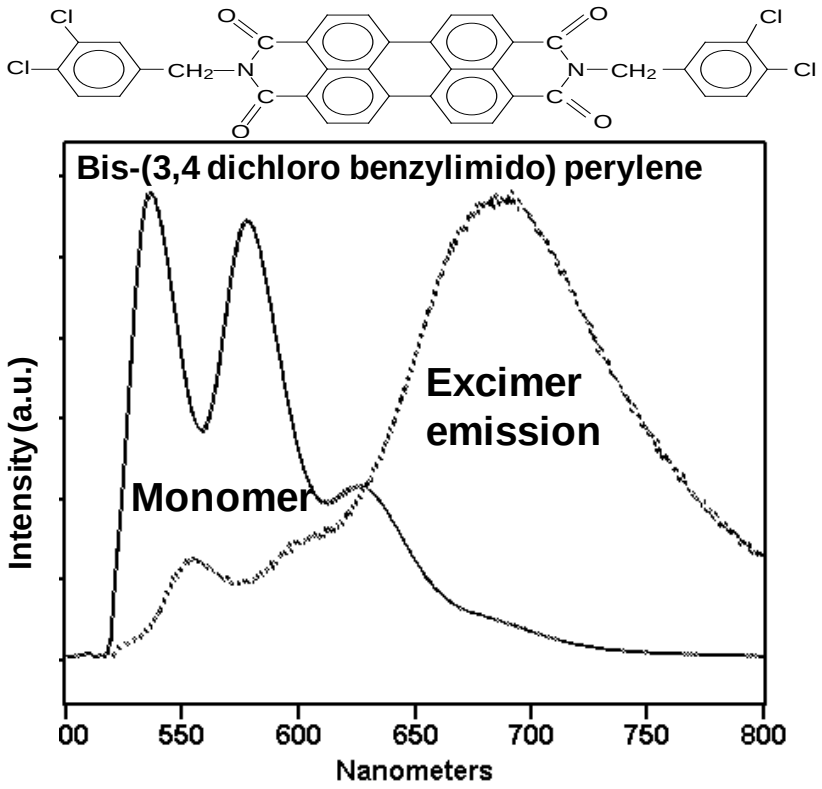

Figure 4.3 PTCD fluorescence spectra for solution and LB monolayer.

It has been previously reported[10], that PTCD derivatives in concentrated solution are known to have distinct emitters, the monomer, and the excimer, which appears in aggregated samples featured in the 1-10 mixed LB monolayer, and it has a broad hump with a maximum around 700 nm, the monomer does appear in the mixed LB, but is more vivid in diluted solution emission.

The frequencies of the monomer and excimer emission are different. The first nanostructure we used was the large spherical Au-SHIN with a plasmon region of 500-600 nm. These nanoparticles will absorb and scatter around this region, and should couple to the emission dipole in this region. Figure 4.4 shows the enhancement results using Au-SHIN spheres and rods. It is clearly seen that only the monomer emission is enhanced

when the Au-SHIN spheres are casted on the sample. In the case of Au-SHIN rods, we observe a drastic change in the spectral profile of the PTCD emission, where the enhancement is now geared toward the excimer emission. The enhancement resulting from the Au-SHIN rods reflects the plasmon profile of the SHIN themselves.

The enhancement spectra are average spectra as it has been taken with a 20X objective lens which covers a 20 μm^2 area.

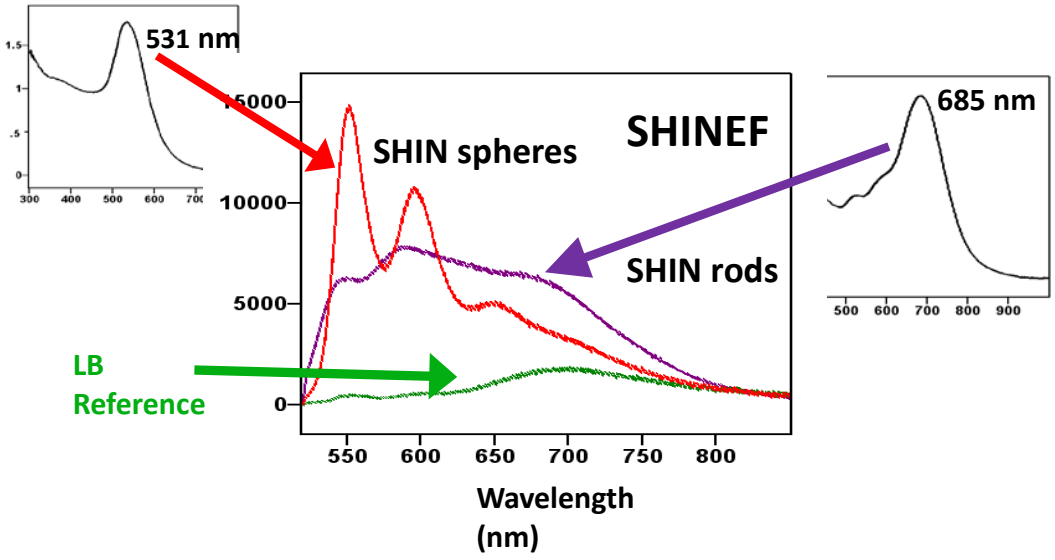

Figure 4.4 Spectral Profile Modification in PTCD mixed monolayer using SHIN spheres and SHIN rods

Figure 4.5 shows the several points of the spherical Au-SHIN mapping. Selective enhancement for the monomer could be seen, and it is a result of the Au-SHIN scattering which is resonating around the monomer region. The LB reference emission is also plotted and it features the excimer peak. It is also evident that the enhancement results are very uniform as they all show the same profile of enhancement which follows the plasmon spectral profile, even in cases where the enhancement is not large.

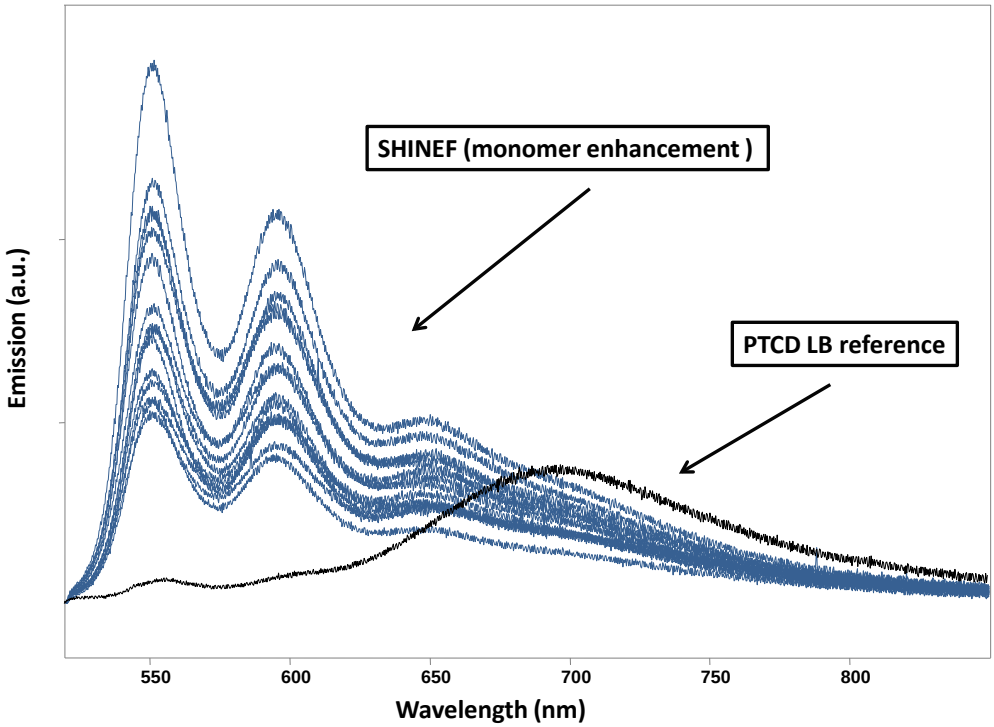

Figure 4.5 Mapping results for SHINEF of PTCD LB monolayer using Au-SHIN spheres

Mapping results for Au-SHIN rods are shown in figure 4.6. Changes in enhancement spectra could be seen following the plasmon profile of the rods.

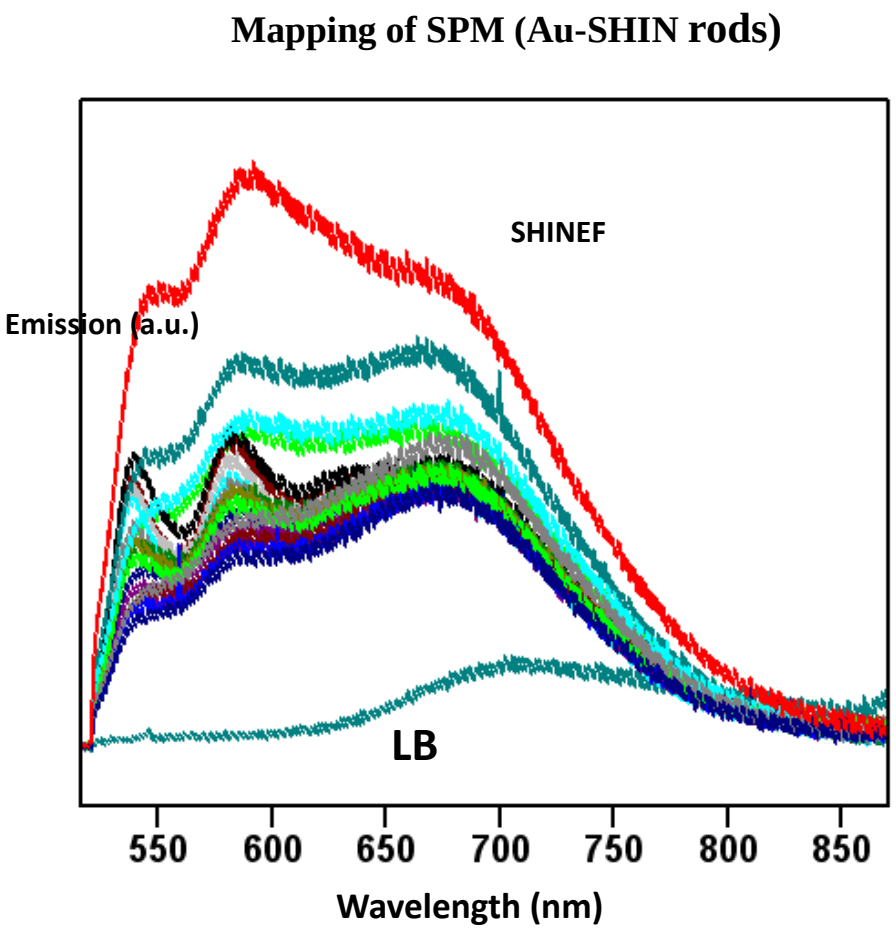

Figure 4.6 Mapping of Au-SHIN rods SHINEF on PTCD mixed LB monolayer

4.4 Conclusion

Spectral profile modification manifests itself as a result of the LSPR interaction with the fluorophore. The radiation of the excited nanostructures dipolar LSPR to the far field carries the signature of the coupled fluorophore emission. We demonstrated the preferential enhancement of the monomer emission in mixed LB monolayer of PTCD, by the use of Au-SHIN spheres resonating in the same range of wavelengths (500-600 nm). When the nanostructure was changed to Au-SHIN rods, for which the plasmon resonates around 650 nm, the excimer emission of PTCD was then preferentially enhanced.

Spectral profile modification notion helps further tailor SEF for cases where preferential enhancement on specific spectral regions is needed.

4.5 References

1. Jackson, J.D., *Classical Electrodynamics*. 3rd Edition ed1999, New York, NY: John Wiley&Sons, Inc.
2. Tam, F., et al., *Plasmonic enhancement of molecular fluorescence.* Nano Lett., 2007. **7**(2): p. 496-501.
3. Le Ru, E.C., et al., *Mechanisms of spectral profile modification in surface-enhanced fluorescence.* Journal of Physical Chemistry C, 2007. **111**(44): p. 16076-16079.
4. Gerstenberg, M.C., et al., *Organic semiconducting thin film growth on an organic substrate: 3,4,9,10-perylenetetracarboxylic dianhydride on a monolayer of decanethiol self-assembled on Au(111).* Physical Review B, 2000. **61**(11): p. 7678-7685.
5. Birks, J.B., *Photophysics of aromatic molecules*1970, London; New York: Wiley-Interscience.
6. Grabar, K.C., et al., *Preparation and Characterization of Au Colloid Monolayers.* Analytical Chemistry, 1995. **67**(4): p. 735-743.
7. Li, J.F., et al., *Shell-isolated nanoparticle-enhanced Raman spectroscopy.* Nature, 2010. **464**(7287): p. 392-395.

8. Nikoobakht, B. and M.A. El-Sayed, *Preparation and growth mechanism of gold nanorods (NRs) using seed-mediated growth method.* Chemistry of Materials, 2003. **15**(10): p. 1957-1962.

9. Gautier, C., et al., *Pigments based on silica-coated gold nanorods: Synthesis, colouring strength, functionalisation, extrusion, thermal stability and colour evolution.* Gold Bulletin, 2010. **43**(2): p. 94-104.

10. Schreiber, F., et al., *Phase-sensitive surface X-ray scattering study of a crystalline organic-organic heterostructure.* Physica B (Amsterdam), 2000. **283**(Copyright (C) 2012 American Chemical Society (ACS). All Rights Reserved.): p. 75-78.

CHAPTER 5

AVERAGE SHINEF AND SHINERS OF HIGH AND LOW QUANTUM YIELD MOLECULES

5.1 Introduction

Surface enhanced fluorescence (or metal enhanced fluorescence) has matured over the last years and research is rapidly expanding to include a broad spectrum of fluorophores as well as enhancing nanostructures with a wide range of applications.

Throughout this thesis, we explored the role of metallic nanoparticles as enhancers for fluorescence emission. Extensive research work has shown that LSPR excitations are the main contributor to the observed enhanced radiation [1, 2]. In addition, the role of the quantum yield of the molecule in the enhancement has been extensively discussed in the literature. Some research work has shown that molecules with low intrinsic quantum yield would get larger enhancement factor from introducing metallic nanoparticles in close proximity to fluorophore. Conversely, molecules with high intrinsic quantum yield may not benefit from the same enhancement [3-5]. High quantum yield dyes are used in fluorescence spectroscopy because even without any enhancement single molecule level detection is achievable, and with the introduction of metallic nanoparticles, photostability of such dyes is improved.[6]

In our work, we utilize a previously developed class of nanoparticles that rise up the sophistication of experimental design in SEF experiment, namely the shell-isolated nanoparticles (SHIN).[7, 8] It has been demonstrated that to achieve SEF, a certain separation between metallic nanoparticle and dyes is required, and SHIN particles provide that. This type of particles increases the practicality and versatility of SEF work, as they could be applied in any kind of solid or solution experiment while obtaining a uniform average enhancement, in additions to that, higher enhancement values –due to hot spots- could also be achieved.[9]

In this chapter, we investigate the role of quantum yield in SEF and examine enhanced fluorescence from molecules with low and high quantum yield.

5.2 Molecular Emission and Its Properties

Molecular emission is quantitatively characterized by the following factors:

$$I_o = I_{exc} \times \varepsilon \times Q_o \quad 5.1$$

Where I_o is the fluorescence intensity, I_{exc} is the excitation intensity, ε is the absorption extinction coefficient, and Q_o is the intrinsic quantum yield.

The quantum yield could also be expressed in terms of lifetime or decay rates as follows:

$$Q_0 = \frac{\Gamma}{\Gamma+\Gamma_{nr}} \quad 5.2$$

Where Γ is the radiative decay rate, and Γ_{nr} is the non radiative decay rate.

Radiative lifetime is the inverse of radiative decay rate

$$\tau = \frac{1}{\Gamma} \quad 5.3$$

While general lifetime of the excited state is the inverse of all measured decay rates

$$\tau = \frac{1}{\Gamma+\Gamma_{nr}} \quad 5.4$$

Upon the introduction of metallic nanoparticles that support LSPR, several changes occur in these parameters. The local electric field surrounding the nanoparticles will be intensified, and as a result, the molecular absorption will be enhanced and in turn so does

the fluorescence. It should be noted that this intense EM field decay with distance from spherical nanoparticle surface according to the following expression:

$\left(\frac{a}{a+d}\right)^6$. Where (a) is the radius of the nanoparticle, and (d) is the distance from the surface of the NP.

In addition, there is a change in the observed lifetimes of the excited state, a reduction in the radiative lifetime which leads to an increase in the radiative decay rates. Just as the nanoparticle provides excitation enhancement, it provides a channel of de-excitation via non-radiative routes which increases the nonradiative decay rate (Γ_{nr}).

The third and perhaps the most important face of enhancement in SEF is the nanoparticle scattering enhancement resulted from coupling of emission to the scattering of the nanoparticles. This effect is discussed in details throughout the thesis as it was the main point of interest in the thesis.

Change in the non-radiative decay rate is done via energy transfer of excitation energy to the electrons of nearby metal, or quenching rate:$\left(\frac{1}{d}\right)^3$, where (d) is as distance from NP surface. Combining this expression with decay of electromagnetic field, one can see that quenching vanishes at a faster rate than the local field enhancement of NP, and as such, resulting fluorescence enhancement is achieved at a certain distance when quenching is almost nonexistent while there is a substantial-enhanced local electric field

Many reports have found that this optimal distance is around 5 nm, where quenching is almost negligible. All published material depicts the trend of fluorescence initial quenching and later enhancement.[10]

In our work, we introduce a spacer layer, a separation between the metal nanoparticle and the fluorophore sufficient to avoid fluorescence quenching and obtain fluorescence enhancement.

5.3 Plasmon Enhanced Fluorescence Enhancement Channels

With this kind of set up, we examine the role of enhancement channels on SEF, utilizing the simplified expression introduced by Halas et al.[11] The nearby nanoparticle will modify the radiative decay rate by a factor χ_r and the quantum yield will be modified as follows:

$$Q_{SEF} = \frac{\chi_r \Gamma}{\chi_r \Gamma + \Gamma_{nr}} \quad 5.5$$

And the intensity of enhanced fluorescence becomes:

$$I_{SEF} = \langle |E|^2 \rangle I_{exc} \times \varepsilon \times Q_{SEF} \quad 5.6$$

In order to evaluate the enhancement, one has to obtain the ratio of SEF to the fluorescence sample:

$$\frac{I_{SEF}}{I_o} = \langle |E|^2 \rangle \frac{I_{exc} \times \varepsilon \times Q_{SEF}}{I_{exc} \times \varepsilon \times Q_o} \quad 5.7$$

By cancelling like terms and expanding the quantum expression, the equation becomes:

$$\frac{I_{SEF}}{I_o} = \langle |E|^2 \rangle \frac{\frac{\chi_r \Gamma}{\chi_r \Gamma + \Gamma_{nr}}}{\frac{\Gamma}{\Gamma + \Gamma_{nr}}} \quad 5.8$$

Rearranging the equation and cancelling like terms gives:

$$\frac{I_{SEF}}{I_o} = \langle |E|^2 \rangle \frac{\chi_r (\Gamma+\Gamma_{nr})}{\chi_r\Gamma+\Gamma_{nr}} \quad 5.9$$

It can be seen that the term χ_r is multiplied by both terms on the numerator while it is multiplied by only the radiative decay rate term in the denominator. There would be an increase in the ratio of the SEF modified quantum yield to the intrinsic quantum yield. This model carries the assumption that the nanoparticle will not affect the molecule non-radiative decay rate by means of energy transfer (quenching), which is indeed the case in our system, where the shell around the nanoparticle (spacer between fluorophore and nanoparticle) is 5-10 nm.

There are two crucial points that should be noted regarding the above expression:

The model shows the effect of the term χ_r , on the quantum yield, but one cannot tell of the magnitude of that effect.

Another crucial point is that χ_r would be relevant for molecules with low intrinsic quantum yield. However, regardless of the magnitude of the enhancement factor, when it comes to high quantum yield molecules, no significance difference would be seen in the expression $\frac{\chi_r (\Gamma+\Gamma_{nr})}{\chi_r\Gamma+\Gamma_{nr}}$ from equation 5.9. There is experimental evidence in published work, including some in this thesis, that SEF is also readily achieved in high quantum yield molecules. This observation supports the notion that the main contribution of enhancement comes from the nanoparticle scattering of the fluorophore emission via dipole coupling.

5.4 Experimental

Low quantum yield dyes were made into aqueous solutions by dissolving the solid (purchased from Sigma Aldrich) in milli Q water. Crystal violet ($C_{25}H_{30}N_3Cl$) was made into stock solution of $1.2*10^{-4}$ M. 100 uL of this stock solution was placed in a quartz cuvette, and diluted to 1 mL with water, thus making the final concentration $1.2*10^{-5}$; this sample served as the blank. For the enhancement experiments, SHIN particles are added to a volume of the 100 uL of dye, and then the volume was complete to 1 mL total, same as the blank, to keep the dye concentration constant throughout the experiments. Varying amounts of SHIN were added in separate trials to determine the best achievable enhancement.

Ethyl violet ($C_{31}H_{42}N_3Cl$) and malachite green ($C_{23}H_{25}N_2Cl$) experiments were done the same way with final concentrations $1.28*10^{-5}$ M and $2.19*10^{-5}$ M respectively.

All SHIN particles were synthesized according the method described in section 3.2.2, and centrifuged prior to use.

The liquid lens attachment was used in the InVia system. The laser power was kept constant throughout the measurements, and both reference and enhanced spectra were recorded during the same session to avoid any instrumental fluctuations.

The LB experiments were carried out for octadecyl rhodamine B chloride (R18) and chromeo 642 carboxylic acid. The mixed spreading solutions contain arachidic acid (AA) and the dye dissolved in chloroform with 1-10 (dye-AA) ratio. The solvent was left to evaporate for 30 minutes and compression of films was done at a constant pressure of 26 $mN.m^{-1}$. Transfer of the monolayer onto a pre cleaned corning 2048 microscope glass

slides was done using Z type deposition. 2 uL of centrifuged shin particles were deposited on a section of the LB slide and left to air dry, prior to spectral measurements.

UV-Vis absorption was recorded using Cary scan 20 UV-Vis spectrometer. SEM images were obtained using the FEI Quanta 200 FEG microscope with an Everhart-Thornley secondary electron detector. TEM characterization was done using FEI Titan 80-300.

5.5 Results and Discussion

5.5.1 Comparison of SHINERS and SHINEF of the Same Molecule.

There were several approaches taken to investigate the role of the fluorophore intrinsic quantum yield. The first approach in our investigation was by examining enhanced fluorescence and Raman scattering of a set of triphenylmethane dyes (crystal violet, and ethyl violet) and a triarylmethane dye (malachite green). These dyes are characterized by their low quantum yield values, below 0.019[12]. Due to their low quantum yield values, the dyes are advantageous for use in our work, because Raman scattering will be apparent without any obscuring from fluorescence background. Shell-isolated nanoparticle-enhanced Raman scattering (SHINERS) and shell-isolated nanoparticle-enhanced fluorescence (SHINEF) with SHINs are essential in shedding light on the role of local field enhancement and also quantum yield in enhanced fluorescence.

The plasmon absorption spectrum of Ag-SHIN, the absorption spectrum of crystal violet, and ethyl violet are shown in Figure 5.1

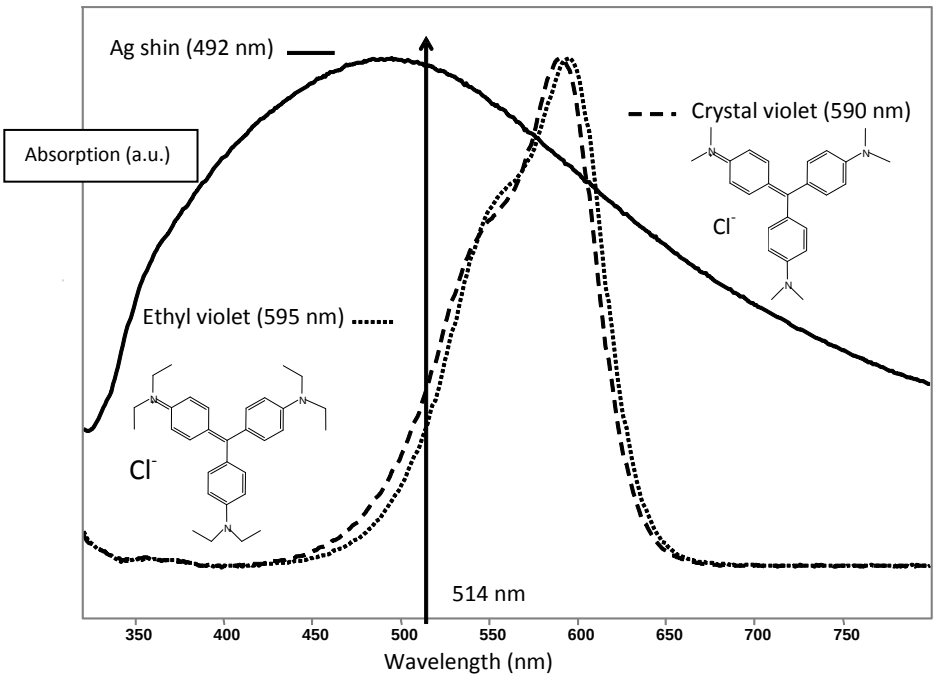

Figure 5.1 Plasmon absorption spectrum of sodium citrate reduced Ag-SHIN, crystal violet, and ethyl violet.

Figure 5.2 shows the SEM characterization for the Ag-SHIN prepared by sodium citrate reduction method. Colloidal Ag (fig 5.2 A) are shown with a polydisperse distribution. (fig 5.2 B,C) images show the Ag-SHIN with the core-shell construction. Scale bar is left to right: 500, 200, and 100 nm.

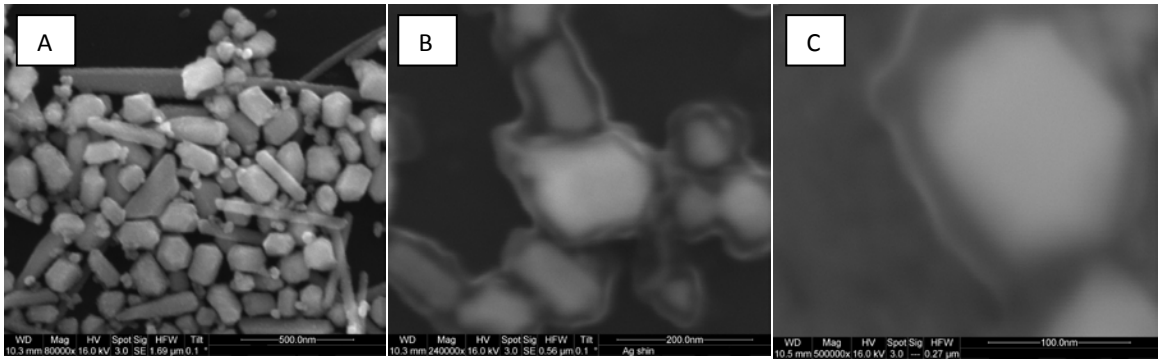

Figure 5.2 SEM images of (A) Ag colloids, and (B, C) SHIN.

The same Ag-SHINs were also characterized by TEM and their images are shown in Figure 5.3. The images show the particles wide distribution in shape and size. Scale bar is 100, 50, 50 nm (L-R).

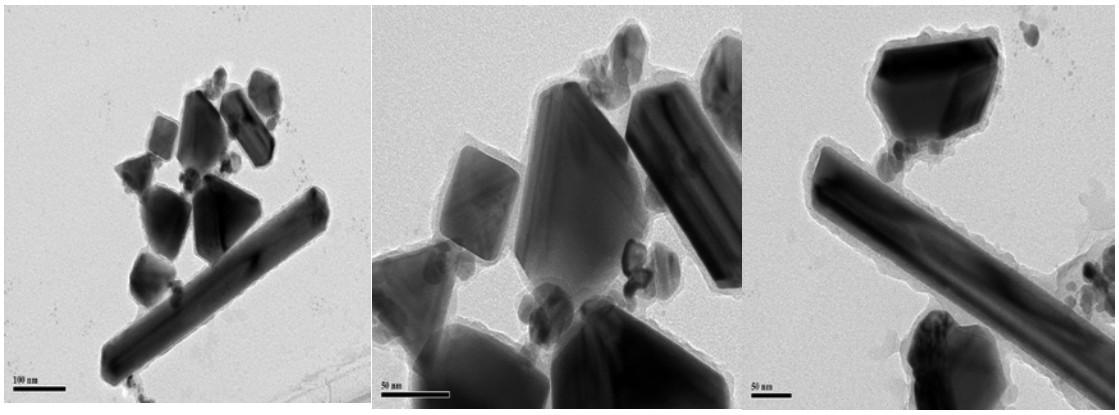

Figure 5.3 TEM images of Ag-SHIN.

Figure 5.4 shows the results of enhancement with ethyl violet and Ag-SHIN (made with citrate reduction method.

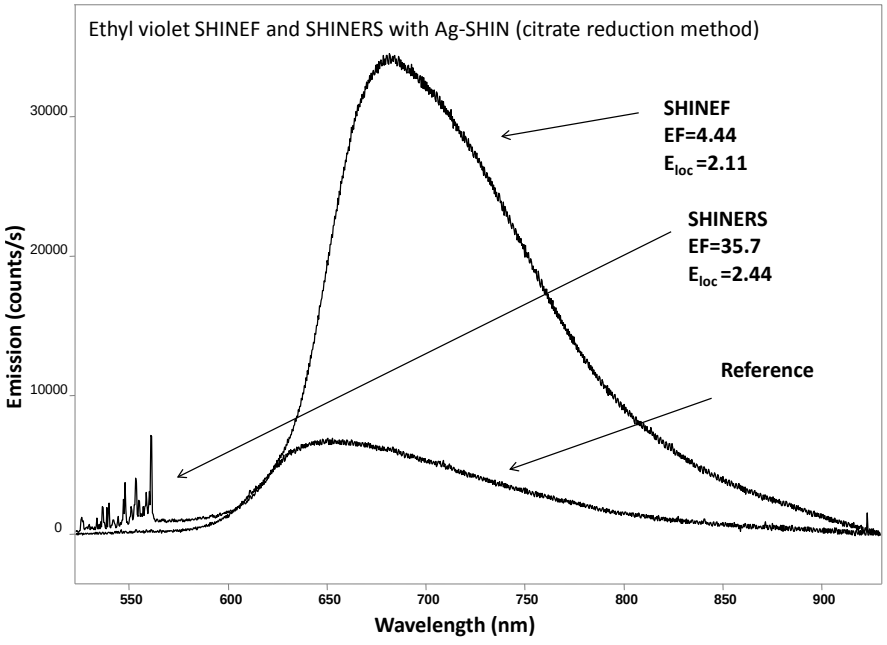

Figure 5.4 SHINERS and SHINEF of ethyl violet with Ag-SHIN.

Both the fluorescence and resonance Raman scattering are enhanced, and enhancement factors are (4.44) and (35.7) for SHINEF and SHINERS respectively. In these measurements, we are working with shell thicknesses where quenching is negligible. The theory predicts three sources of enhancement for fluorescence, enhancement in absorption, enhancement in radiative decay rate, and NP scattering enhancement. The fluorophores used here are ideal in the sense that they show both fluorescence and resonance Raman within the same spectrum. Of course, enhanced absorption and enhanced radiative decay rate affect only the fluorescence.

However in our results, it can be seen that the fluorescence enhancement factor is the square value of the electric field while the enhanced resonance Raman is the fourth power of the same field, which is consistent with the theory[13] , and supports the role of the local field in the enhancement, which here is mainly due to the nanoparticle scattering of the fluorophore emission,

Local field enhancement calculations confirm the notion that when it comes to enhancement, the nanoparticle local field plays the main role, Theoretical calculations of the local electric field (introduced in Figure 1.2) are in good agreement with the values presented experimentally here for Ag-SHIN with a shell around 10 nm. For completeness, we revisited the crystal violet results[14] using the new Ag-SHINs and the results were in full agreement with those obtained for ethyl violet. Figure 5.5 shows SHINERS and SHINEF of crystal violet with the new Ag-SHINs.

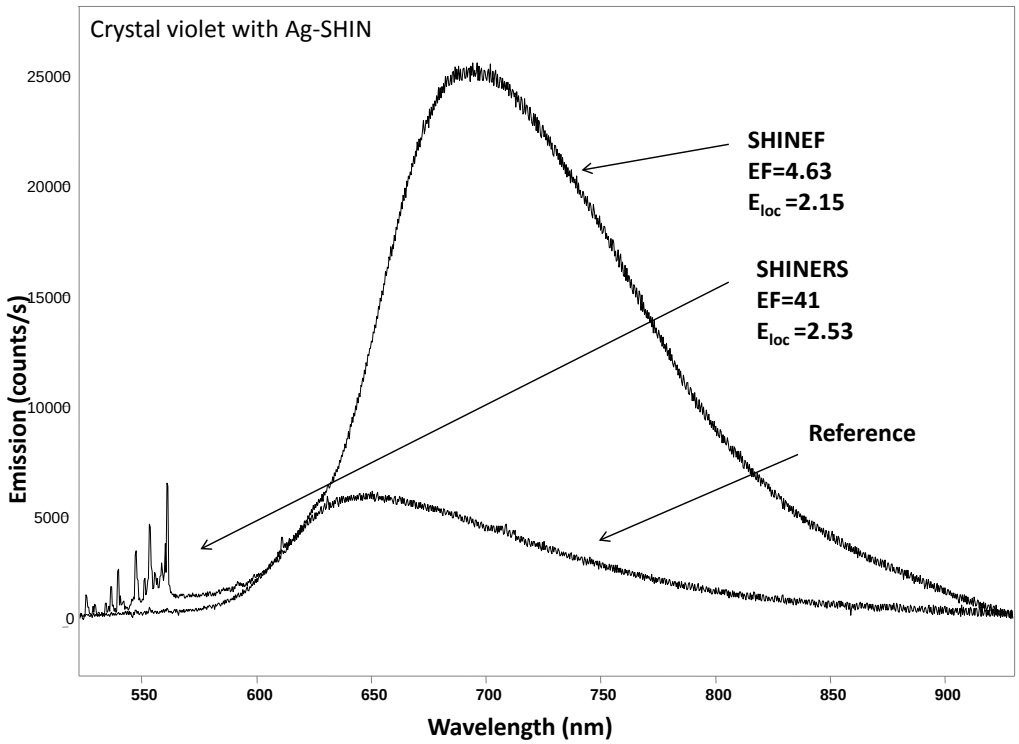

Figure 5.5 SHINERS and SHINEF of crystal violet with Ag-SHIN.

The experiment was repeated with Ag-SHINs synthesized via reduction of silver salt with hydroxyl amine. Figure 5.6 (A) shows SEM and (B) TEM images for these particular Ag-SHINs particles

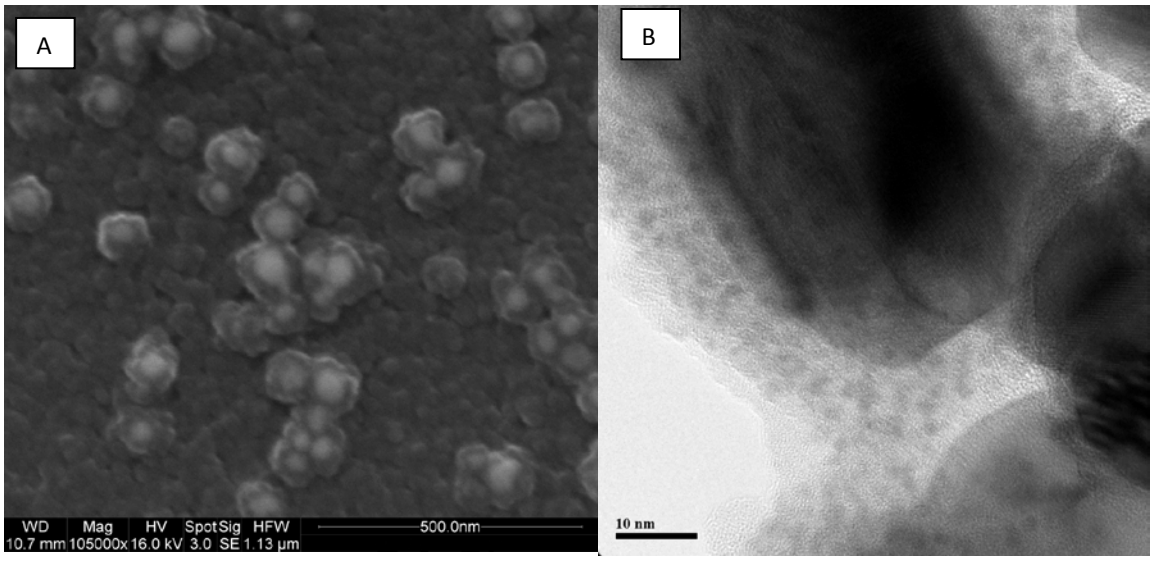

Figure 5.6 (A) SEM and (B) TEM images Ag-SHIN (reduced with hydroxyl amine).

Enhancement results with these Ag-SHINs for both dyes show that both SHINEF and SHINERS produce nearly the same local electric field value. SHINEF and SHINERS of crystal violet with Ag-SHIN is shown in figure 5.7 (A), and ethyl violet results are shown in figure 5.7(B)

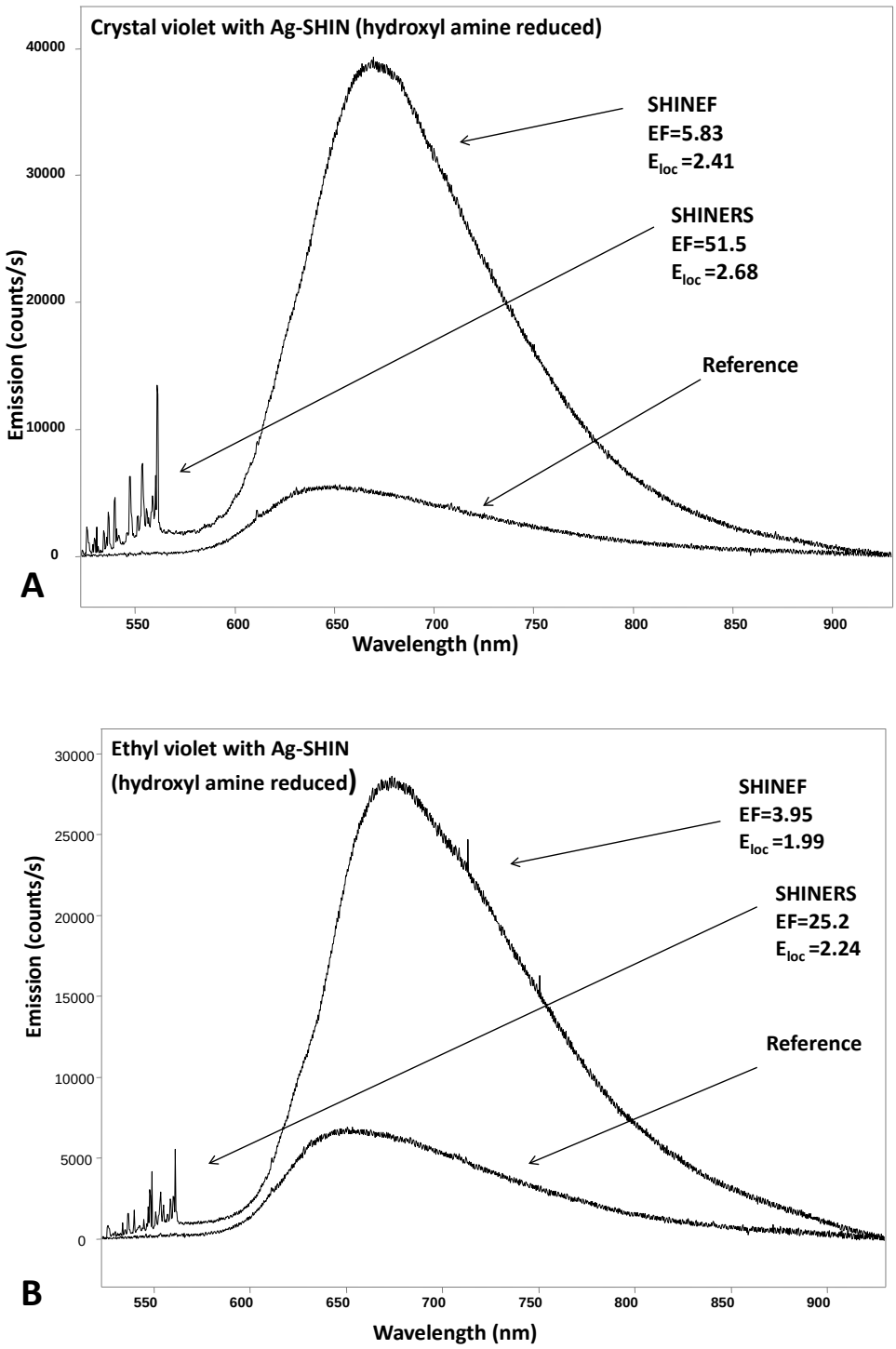

Figure 5.7 SHINEF and SHINERS of (A) crystal violet and (B) ethyl violet using Ag-SHIN (reduced using hydroxyl amine)

Similar experiments were carried out using gold nanoparticles (Au-SHINs) instead of silver. The theoretical calculation for local field enhancement of Au-SHINs with 40 nm Au core and 11 nm SiO_2 shell, expressed as$(\frac{|E|^2}{|E_0|^2)}$ are shown in figure 5.8[15]

Figure 5.8 Theoretical calculations for the enhanced local electric field of an Au-SHIN. Adapted from Aroca, R.F., et al. 2011.

Figure 5.9 shows the absorption spectra of ethyl violet and Au-SHINs. Enhancement results are displayed in figure 5.10; and it can be seen that both SHINEF and SHINERS agree with theoretical calculations of Au-SHINs. Enhancement values are lower relative to Ag-SHIN because the enhanced electric field is lower in case of Au-SHINs.

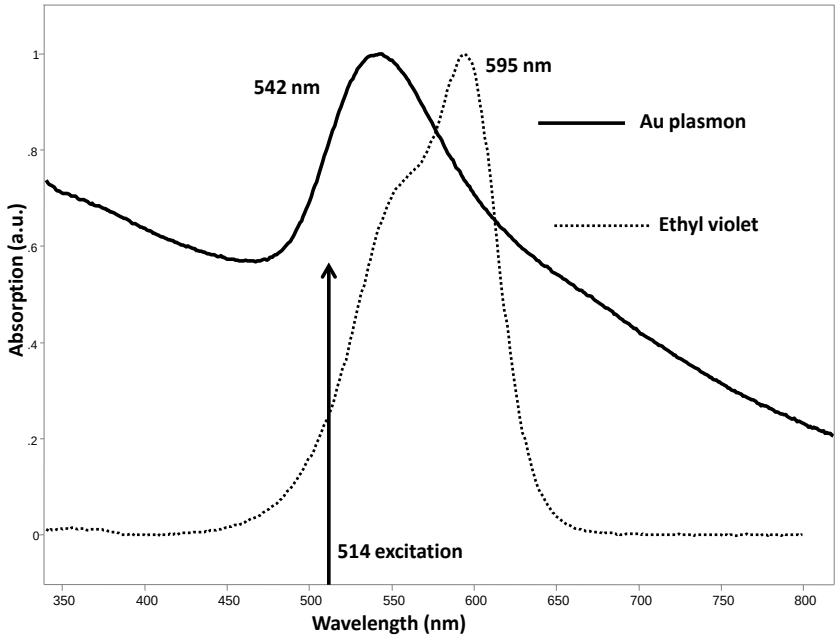

Figure 5.9 absorption spectra of Au-SHINs and ethyl violet.

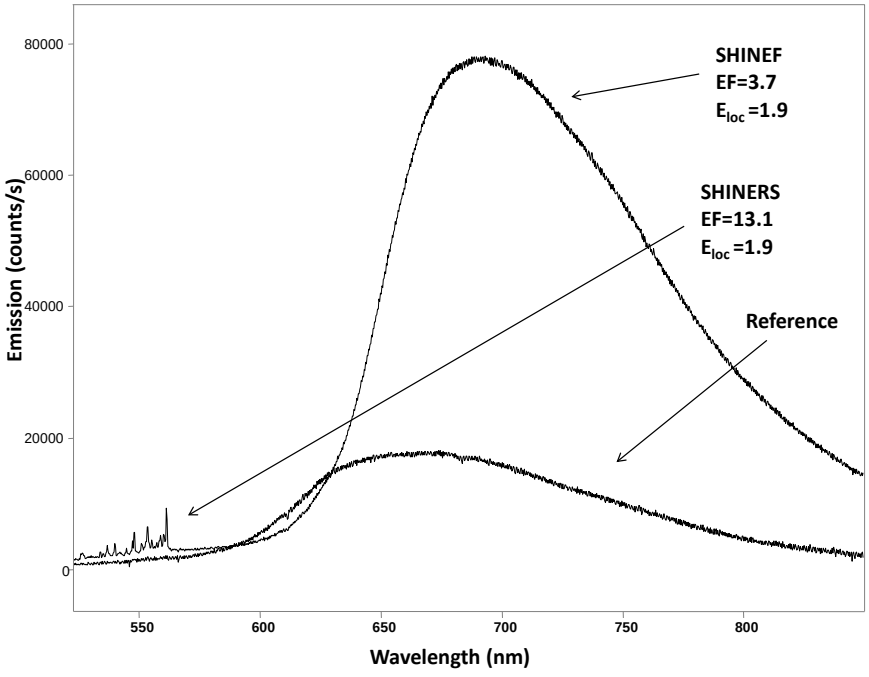

Figure 5.10 SHINEF and SHINERS of ethyl violet solution using Au-SHINs (citrate reduction method).

The SHINERS and SHINEF results show that in these experiments of average enhancement, both the scattering and the emission equally benefit from the local electric field enhancement. If one assumes that there is a considerable contribution from enhanced absorption or enhanced radiative decay rate, SHINEF and SHINERS would not lead to same values for the local electric field enhancement. In addition, to a large extent there is a good agreement with the theoretical calculations of electric local field outside these SHINs enhancers.

5.5.2 Fluorescence-plasmon Overlap

Here, we further examine the role of the fluorophore quantum yield and nanoparticle plasmon in the observed SHINEF enhancement using the molecule of malachite green.

Malachite green is the molecule of choice since it has a very similar structure to ethyl violet and crystal violet, however the absorption and emission of malachite green is red shifted relative to the other dyes, which makes it an ideal candidate to be examined with two different excitation laser lines: 514 nm and 632.8 nm.

The SHIN's plasmon should be broad enough, and can be excited by either of these two lasers. These requirements are fulfilled with Ag-SHIN synthesized with sodium citrate method. In figure 5.11, the absorption spectra of malachite green, Ag-SHINs and emission spectrum of malachite green are all normalized and displayed in relation to the two excitation sources used 514nm laser, and 632.8 nm laser.

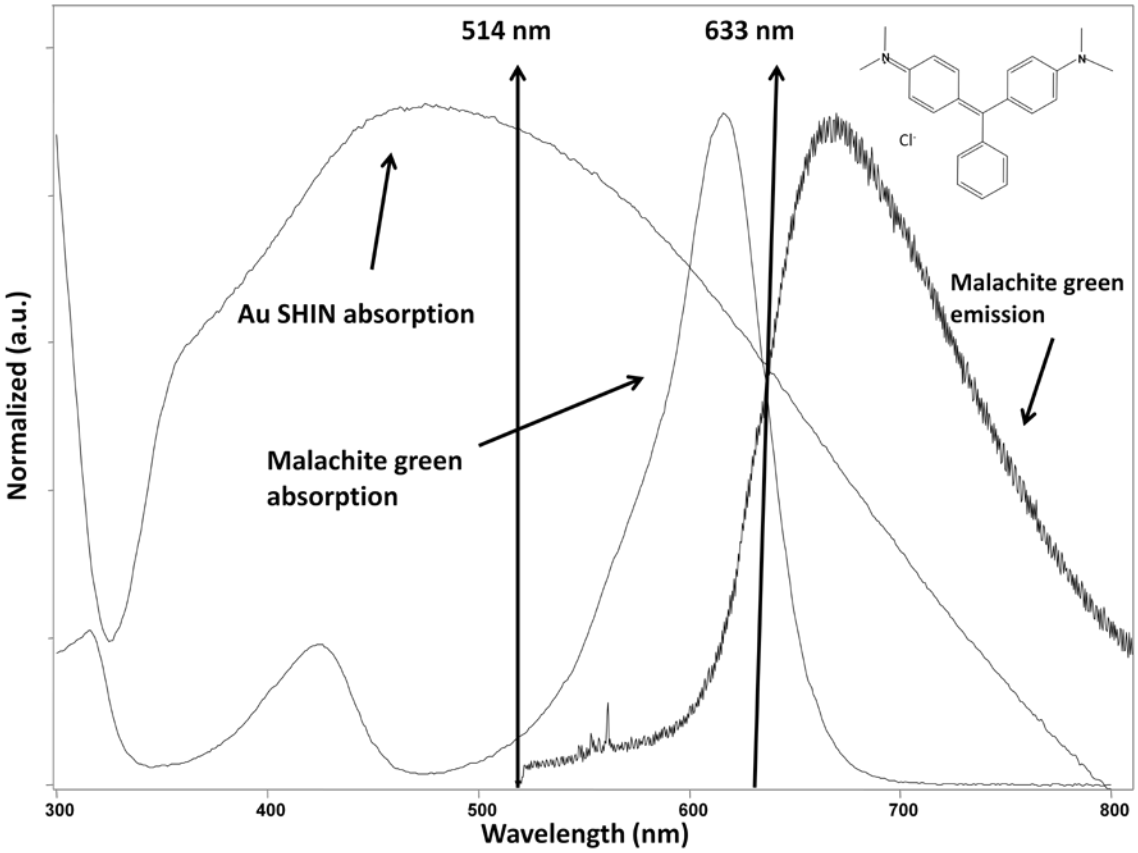

Figure 5.11 Malachite green absorption and emission and Ag-SHIN (citrate reduction method).

Figure 5.12 shows the enhancement results for malachite green with Ag-SHIN using 632.8 nm laser excitation; we can see both SHINEF and SHINERS. Area under peaks fitting shows that both enhancements give very similar values for the electric field, which means that nanoparticles with plasmon around 633 nm excitation are responsible for this enhancement.

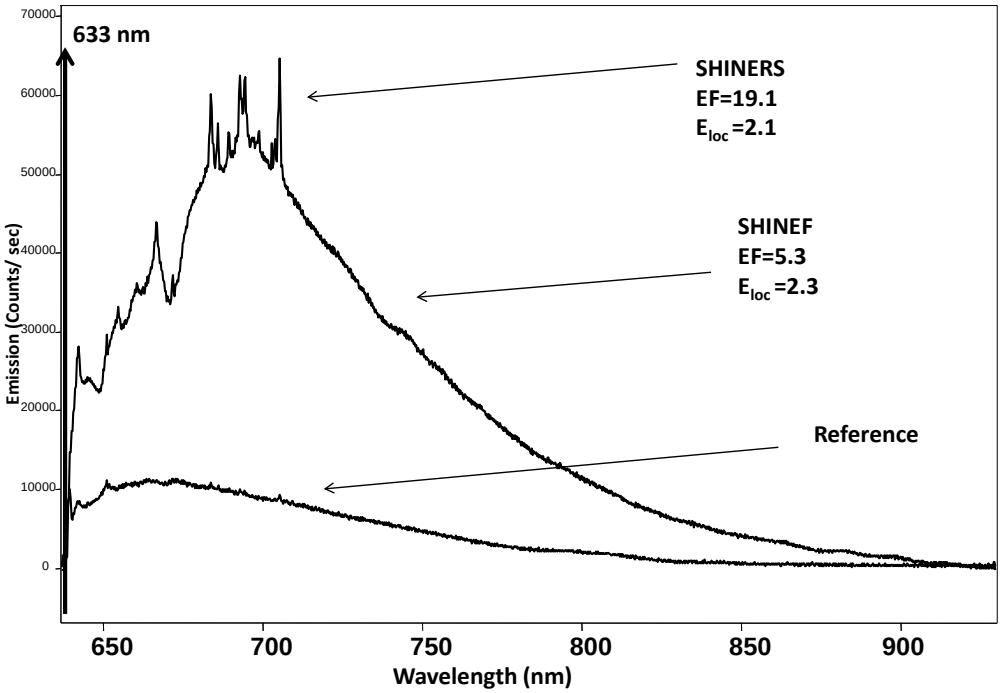

Figure 5.11 SHINEF and SHINERS of malachite green using Ag-SHIN with 633 nm laser.

Notably, when we employ a laser line with higher energy (514 nm laser line), different population of nanoparticles are excited, precisely, those nanoparticles absorbing and scattering around 514 nm. It is important to point out here that to maximize the emission enhancement it is necessary to match the spectral region of nanoparticle scattering and fluorescence emission. Therefore, the change in the laser line will affect the matching of the nanoparticle scattering of the fluorophore emission. At 514 nm, the excited plasmon could dipole couple with emission that is in the same spectral region, however; malachite green emission is to the red of the excited plasmon.

Figure 5.13 shows the enhancement results of Ag-SHIN with malachite green using 514 nm laser line. Only minimal fluorescence enhancement could be seen (EF=1.4), however; Raman scattering enhancement factor is still clearly observed.

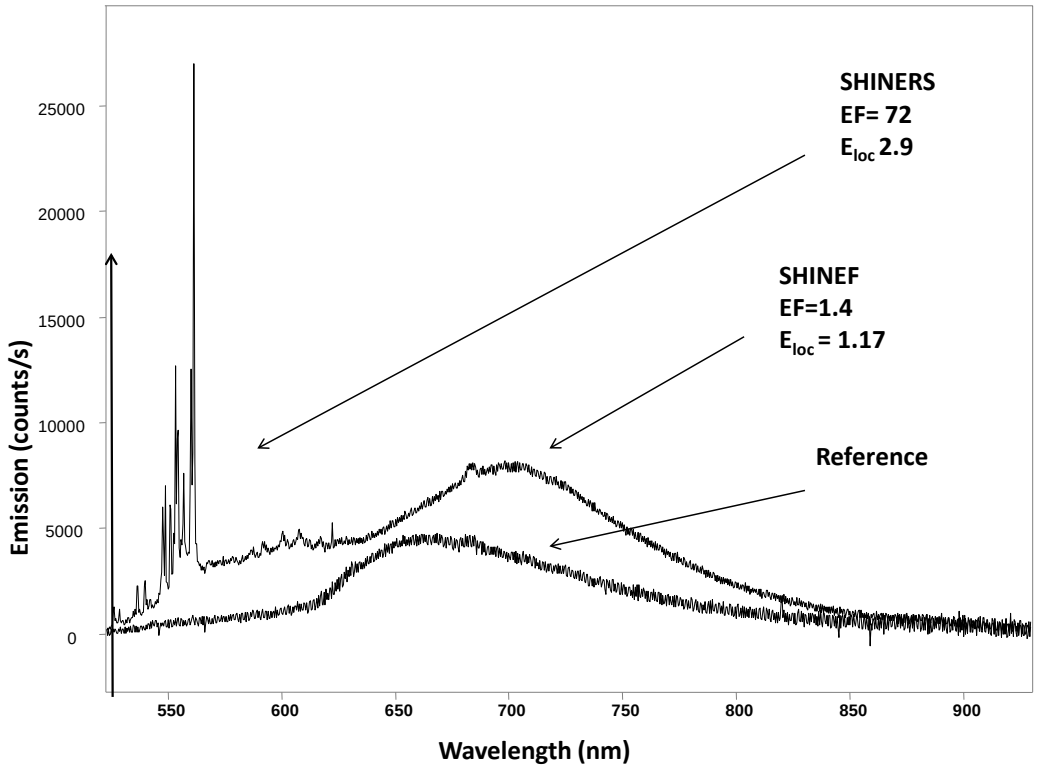

Figure 5.12 Enhancement results for malachite green and Ag-SHIN using the 514 nm excitation source.

The Ag-SHINs are still performing their role enhancing the Raman scattering, which follows the excitation energy, in other words, the overlap between the Raman scattering and nanoparticle scattering is met. However, due to the spectral mismatch between the emission and active plasmon around 514 nm, there was little enhancement in

fluorescence. Since malachite green is a low quantum yield probe, the results seems to suggest that when it comes to enhanced fluorescence, quantum yield plays a minimal role, and that determining contribution comes from Ag-SHINs, that captures the molecular emissions and re-radiates it to the far field where it can be detected.

5.5.3 Enhanced Emission from LB Monolayers

We further investigate the role of quantum yield in SHINEF by direct comparison of enhancement obtained with Ag-SHIN dispersed onto LB monolayers of two molecules with different quantum yield values.

The two dyes used here are octadecyl rhodamine B chloride (R18) which has a high quantum yield value of 70%[16], and chromeo 642 carboxylic acid which has a 17 % quantum yield value.[17] Using here the Langmuir-Blodgett technique provides important advantages:

In comparison to solutions, the dye charge, and how it interacts with the Ag-SHIN surface charge, is not longer a dominant factor; this will ensure that two different dyes in charge and chemical structure will have the same close proximity to the Ag-SHIN particles. The Ag-SHINs are casted so the only separation between the nanoparticles and the dye molecules is the silica shell, which could be controlled better.

Figures 5.13 shows the enhancement results of casting two drops from the same batch of Ag-SHIN on an LB of R18 (figure A)and chromeo 642 (figure B) monolayers.

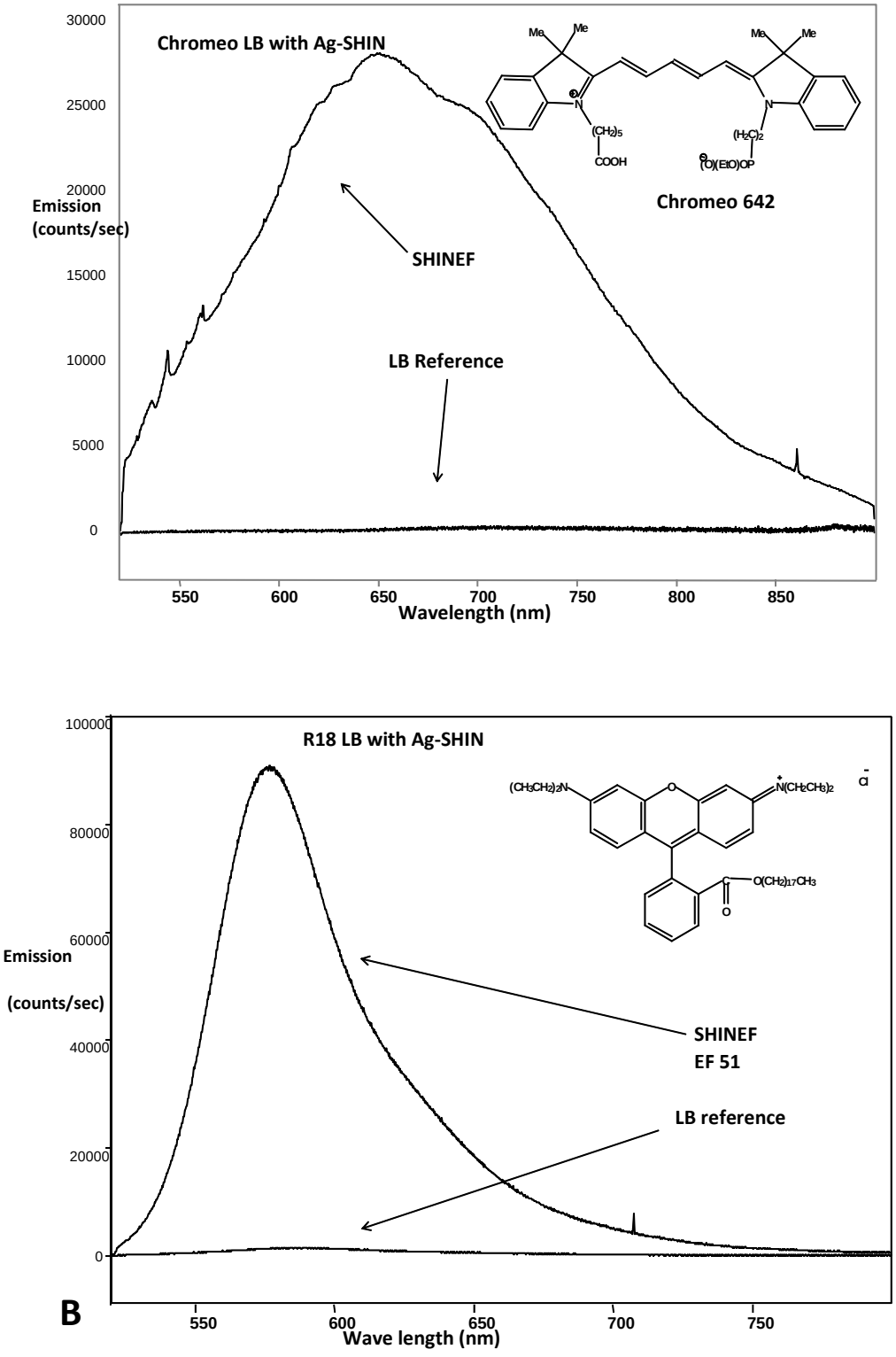

Figure 5.13 SHINEF of (A) chromeo 642 and (B) R18 with Ag-SHIN.

A mapping of many points was taken for each sample to get an average of the enhancement factor. The enhancement factor in each of the LB monolayers varied across the sample, which is normal considering a formation of areas of highly intense electric fields in Ag-SHIN aggregates (plasmon coupling), in these hot spots, enhancement factors would be higher than the previous set of results in solution experiments.

An accurate comparison between the two dyes should consider taking many points, examine the general trend of enhancement, and look at the highest enhancement achievable in each set of results. In the case of R18, the highest EF attainable was 51, while in the Chromeo 642 case, it was 53. These two EF values should be very different had there been a substantial role for intrinsic quantum yield value in enhancement.

5.6 Conclusion

Plasmon enhanced fluorescence benefits from enhancements in absorption, increase in radiative decay rate, and enhanced emission by coupling to a scattering nanoparticle. In the set of experiments presented here for average SHINEF in solution and LB monolayers, it is found that the most important contributing factor is the re-radiation of the fluorophore emission, and also that intrinsic quantum yield plays minimal role. This challenges the common belief that enhancement factor is inversely proportional to intrinsic quantum yield of the fluorophore. These average results are not to be extended to specific work recently carried out on isolated hotspots.

We have confirmed for low quantum yield molecules in solution and different Ag-SHINs (and Au-SHINs) that enhanced fluorescence (E^2) and enhanced Raman scattering (E^4)

are proportional to local electric field (E) values. Had there been a substantial role to quantum yield in enhancement, fluorescence enhancement would be higher than the square of the electric field extracted from SHINERS. We also show that maximum enhancement factors attained in LB monolayers of high quantum yield and low quantum yield molecule in LB monolayers are very similar. The latter also supports the suggestion that the enhancement mainly as a result of the nanoparticle scattering of fluorophore emission.

5.7 References

1. Le, R.E.C., et al. *Spectral profile modifications in metal-enhanced fluorescence*. 2010. John Wiley & Sons, Inc.
2. Rubim, J.C. and R.F. Aroca, *The observation of high order overtones and combinations in the SERRS spectra of a perylene dye spin coated onto silver island films.* Phys. Chem. Chem. Phys., 2008. **10**(Copyright (C) 2012 American Chemical Society (ACS). All Rights Reserved.): p. 5412-5418.
3. Bardhan, R., N.K. Grady, and N.J. Halas, *Nanoscale control of near-infrared fluorescence enhancement using Au nanoshells.* Small, 2008. **4**(Copyright (C) 2012 American Chemical Society (ACS). All Rights Reserved.): p. 1716-1722.
4. Gill, R. and R.E.C. Le, *Fluorescence enhancement at hot-spots: the case of Ag nanoparticle aggregates.* Phys. Chem. Chem. Phys., 2011. **13**(Copyright (C) 2012 American Chemical Society (ACS). All Rights Reserved.): p. 16366-16372.
5. Weitz, D.A., et al., *The enhancement of Raman scattering, resonance Raman scattering, and fluorescence from molecules adsorbed on a rough silver surface.* J.

Chem. Phys., 1983. **78**(Copyright (C) 2012 American Chemical Society (ACS). All Rights Reserved.): p. 5324-38.

6. Lakowicz, J.R., *Principles of fluorescence spectroscopy*1983, New York: Plenum Press.
7. Li, J.F., et al., *Shell-isolated nanoparticle-enhanced Raman spectroscopy.* Nature, 2010. **464**(7287): p. 392-395.
8. Guerrero, A.R. and R.F. Aroca, *Surface-Enhanced Fluorescence with Shell-Isolated Nanoparticles (SHINEF).* Angew Chem Int Ed Engl, 2010(Copyright (C) 2012 U.S. National Library of Medicine.).
9. Moula, G. and R.F. Aroca, *Plasmon-Enhanced Resonance Raman Scattering and Fluorescence in Langmuir-Blodgett Monolayers.* Anal. Chem. (Washington, DC, U. S.), 2011. **83**(Copyright (C) 2012 American Chemical Society (ACS). All Rights Reserved.): p. 284-288.
10. Anger, P., P. Bharadwaj, and L. Novotny, *Enhancement and Quenching of Single-Molecule Fluorescence.* Phys. Rev. Lett., 2006. **96**(11): p. 113002-1 to 113002-4.
11. Bardhan, R., N.K. Grady, and N.J. Halas, *Nanoscale Control of Near-Infrared Fluorescence Enhancement Using Au Nanoshells.* Small, 2008. **4**(10): p. 1716-1722.
12. Brey, L.A., G.B. Schuster, and H.G. Drickamer, *High pressure studies of the effect of viscosity on fluorescence efficiency in crystal violet and auramine O.* The Journal of Chemical Physics, 1977. **67**(6): p. 2648-2650.
13. Le Ru, E.C. and P.G. Etchegoin, *Rigorous justification of the E (4) enhancement factor in Surface Enhanced Raman Spectroscopy.* Chemical Physics Letters, 2006. **423**(1-3): p. 63-66.

14. Guerrero, A.R., Y. Zhang, and R.F. Aroca, *Experimental Confirmation of Local Field Enhancement Determining Far-Field Measurements with Shell-Isolated Silver Nanoparticles.* Small, 2012. **8**(Copyright (C) 2012 American Chemical Society (ACS). All Rights Reserved.): p. 2964-2967.

15. Aroca, R.F., et al., *Plasmon-Enhanced Fluorescence and Spectral Modification in SHINEF.* The Journal of Physical Chemistry C, 2011. **115**(42): p. 20419-20424.

16. Crosby, G.A. and J.N. Demas, *Measurement of photoluminescence quantum yields. Review.* J. Phys. Chem., 1971. **75**(Copyright (C) 2012 American Chemical Society (ACS). All Rights Reserved.): p. 991-1024.

17. Wetzl, B., et al., *Set of fluorochromophores in the wavelength range from 450 to 700 nm and suitable for labeling proteins and amino-modified DNA.* Journal of Chromatography B, 2003. **793**(1): p. 83-92.

CHAPTER 6

A METHOD FOR APPLYING SHIN PARTICLES

6.1 Introduction

One of the ultimate goals for spectroscopic techniques used for detection is to increase their sensitivity and thus their efficiency. In SERS and SEF the ultimate sensitivity is achieving single molecule detection. While this level has been achieved in many reports [1-4], there are still many challenges that face trace detection analysis in general; one is the low probability of finding hot spots, areas of extreme enhancement required for SMD.

6.2 Hot Spot

Hot spot is the term coined for areas in nanoparticle aggregates, specifically in the vicinity between two adjacent nanostructures. In addition to enhanced local electric field from individual nanoparticle plasmon, there would be further increase due to the coupling between two or more nanoparticles' plasmon. The coupled plasmon display a more intense localized electric field that is responsible for up to 10^{10} enhancement[5]. The coupled LSPR excitation is highly localized, with such high enhancement values available only to molecules located exactly between two nanostructures, nonetheless the closer the molecules are to the hot spot site the stronger the enhancement it experiences.

Highly controlled nanostructure arrangements are essential to construct plasmon coupling sites. One obstacle remains, and that is the limitation of such structures to be utilized in real world application. [6, 7]

We see the need for an affordable, easy method to facilitate plasmon coupling and increase the probability of creating hot spots and, at the same time, increasing the average enhancement factor. The nature of shell-isolated nanoparticle provides a great deal of

versatility in experimental design. They could be used as enhancing nanostructure in solution, or could be applied on any kind of surface regardless of surface morphology and composition. Targeting that aspect of the SHIN particles is our aim in this chapter. Casting of SHIN particles is an easy process and is already proven to be very useful in surface enhanced spectroscopy theoretical studies and application likewise. [3, 8, 9]

However, SHIN casting is done by dropping the solution on surfaces, so the distribution of the SHIN particles is random, and there could be areas with high concentration of SHIN while other areas are lacking of enough number of SHIN to ensure good enhancement. Figure 6.1 shows the inhomogeneity within a single small drop cast.

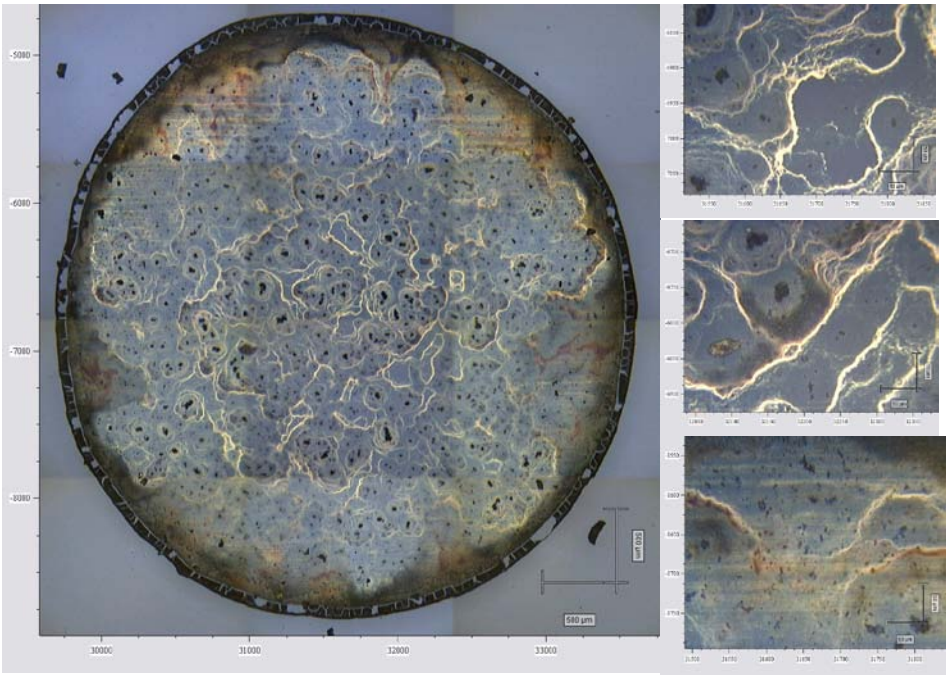

Figure 6.1 SHIN drop cast under a light microscope. Image is taken by author.

The image to the left is the whole drop taken with a 5X objective (scale bar is 500 µm, and inset images to the right are sections of the same drop showing an uneven distribution

of SHIN particles, images taken with a 20 X objective lens and the scale bar is50 µm. The dark clusters and bright lines in the figure are both areas of very high concentration of SHINs, while the rest of the drop lacks a sufficient coverage of SHINs.

Here we use manual spraying devices that provide a finer stream of shin solution. This method will provide coverage to the surface with many tiny droplets. Because these droplets are small and cover the whole surface, the nanoparticles will be distributed more evenly and any aggregation due to solvent evaporation will be highly localized within the fine mist droplets.

We employ a sprayer that is commercially available, and affordable, to provide a thin mist of SHIN particles, where we spray glass slides of mixed LB monolayers of octadecyl rhodamine B (R18) to observe the profile of enhancement and contrast it with enhancement obtained by drop casting the same SHIN on same dye.

6.3 Experimental

The SHIN particles were synthesized as outlined in section (3.2.2.2) of this thesis. A pre cleaned sprayer is rinsed with the shin solution prior to use, the shin is sprayed few times to ensure no other contamination is present in the system. LB mixed monolayer of R18 and arachidic acid is prepared by spreading a 250 uL of (1-10) molecular ratio of R18-AA on a Milli Q water-air interface, the solution was left for 30 minutes to ensure complete evaporation of dichloromethane used as the solvent. After solvent evaporation, a set of barriers compressed the floating film to a maximum pressure of 25 mN/m, and pressure is kept constant at this value during transfer. Small cut out pieces of washed Corning glass

slides all attached to a glass micro slide were submerged in the water prior to Langmuir film casting. The micro slide with the small pieces attached was lifted at a 2mm/min speed where deposition was Z type.

After deposition, one piece was set aside to serve as a reference, and 12 other pieces were laid side to side to be sprayed.

The samples were divided into 6 groups of two slides each to vary the number of SHIN sprays. The groups were as follows: 5 sprays, 10 sprays, 15 sprays, 20 sprays, 25 sprays, and 30 sprays.

All pieces laid side to side, shin was applied one spray at a time, the spray was left for 10 minutes to completely dry before next round of coating. After reaching 5 sprays, two pieces were removed, one would be used for fluorescence and UV-Vis measurements, and another used for SEM analysis. Spraying was continued in the same fashion (spray round followed by 10 minutes min drying time), till all six groups finished.

UV-Vis measurements were performed on all glass slides after running the unsprayed R18 LB as a background reference.

SEM measurements were performed using the SEM microscope specified in section (3.3.1); the glass slides were coated with carbon under vacuum to avoid surface charging.

AFM measurements were done on some particles from the same batch. Particles were fixed on glass substrate using the silane coupling agent (APTMS). The chemical treatment and AFM measurements were done with help and supervision of Aisha Alsaleh based on modifications she performed on fixation method used originally on colloids.

AFM sample was prepared as follows: a glass slide was cleaned with aqua regia, washed abundantly with milli Q water, dried and then washed again with acetone. Then it was dipped in a solution of APTMS for 30 minutes, and removed and dipped in the SHIN solution for 16 hours.

6.4 Results and Discussion

6.4.1 Ag-SHIN Characterization

Figure 6.2 shows the absorption the Ag-SHIN, which appears to have a broad plasmon peak (maximum around 406 nm) consistent with this synthesis method, and coincides with R18 fluorescence emission of a mixed LB monolayer (1-10) R18-arachidic acid maximum at about 580 nm.

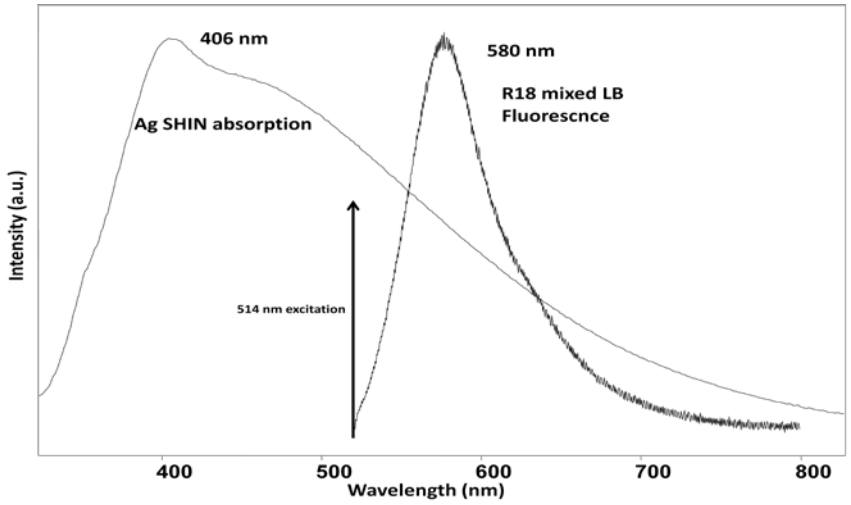

Figure 6.2 Ag-SHIN absorption spectrum imposed over R18 mixed LB emission spectrum.

Figure 6.3 shows the nature of the particles used in this work under SEM microscope, a polydisperse population of colloids is seen in figure 6.3, which is also reflected in the broad plasmon in figure 6.2. Figure 6.3 (left) shows the colloidal particles, and (center and right) images shows the silver core and the surrounding silica shell, the shell measures to be slightly larger than 10 nm, the actual shell would be slightly lower as SEM measurements normally overestimate such features due to the conductive coating on surface and the fact that the images were obtained at such high magnification.

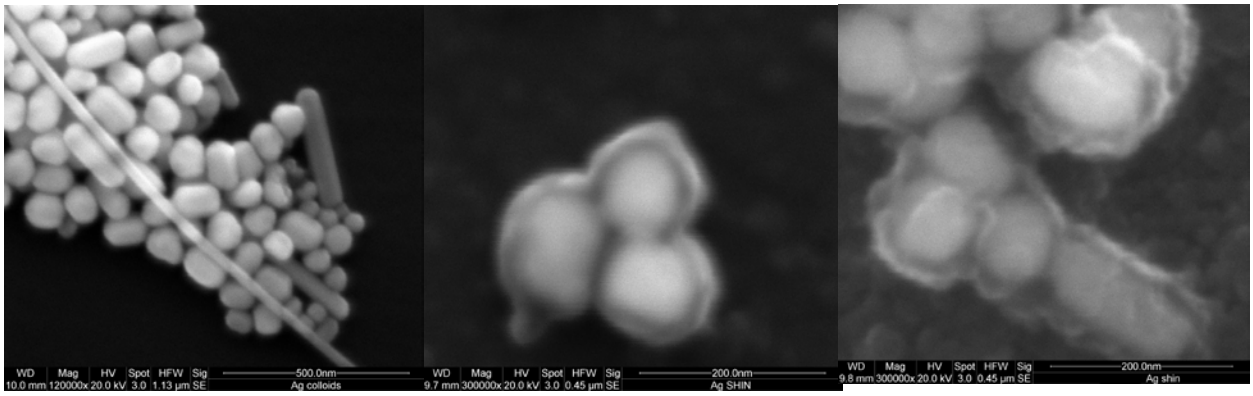

Figure 6.3 SEM images of Ag colloids and SHIN.

AFM images (shown in figure 6.4) show the same polydisperse profile of these particles with particle sized ranging between (50-100 nm). Scale bar is 2 µm for the left image and 500 nm for the right image.

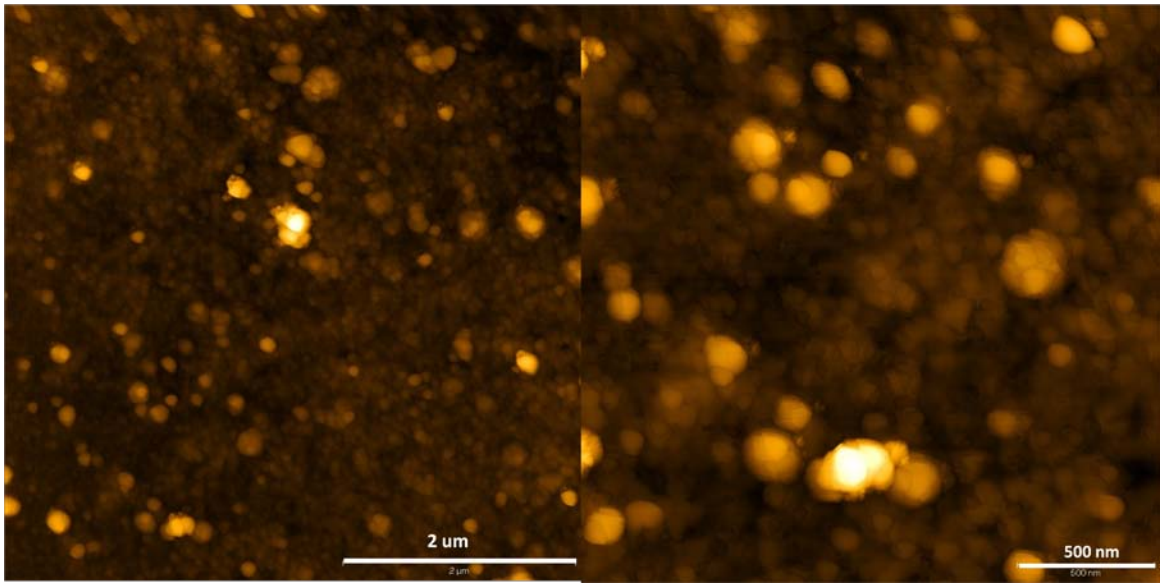

Figure 6.4 AFM images of Ag-SHIN.

By spraying the probed surface with fine mist of SHIN particles, they will be scattered throughout the samples, and will progressively be situated close to other SHIN particles, and thus increase the chances of plasmon coupling. The advantage of this method lies in its ease, as it could be applied to any surface type and morphology, and there is no need for any surface cleaning or chemical treatment prior to SHIN spraying. Figure 6.5 displays a graphical representation of proposed increase of plasmon coupling discussed above.

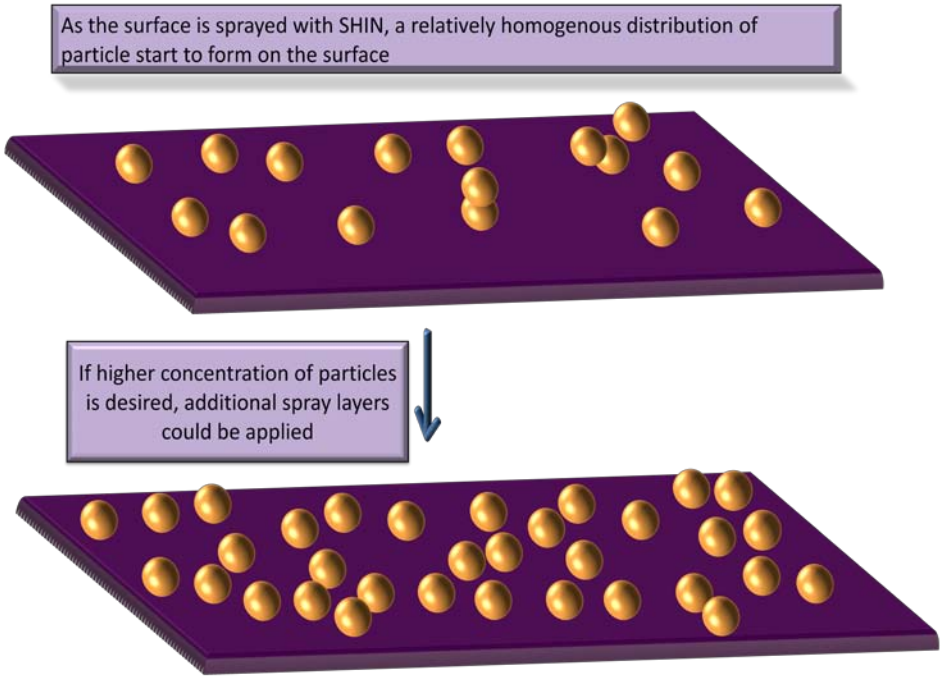

Figure 6.5 Graphical representation of SHIN spraying.

6.4.2 UV-Vis of Spray Samples

As mentioned earlier, there was a total of 6 sets (5, 10, 15, 20, 25, 30 sprays). Absorption measurements were also done on the sprayed glass slides as seen in figure 6.6. Plasmon absorption of Ag-SHIN was not detected even in the most concentrated sample (30 sprays), possibly due to relatively scarce number of nanoparticles to show a plasmon peak in UV-Vis absorption technique. However, there was an increase in the scattering background with increasing spray coatings, all the spectra are displayed with the same scale, which could be indicative of the increasing number of SHIN particles on the glass slides.

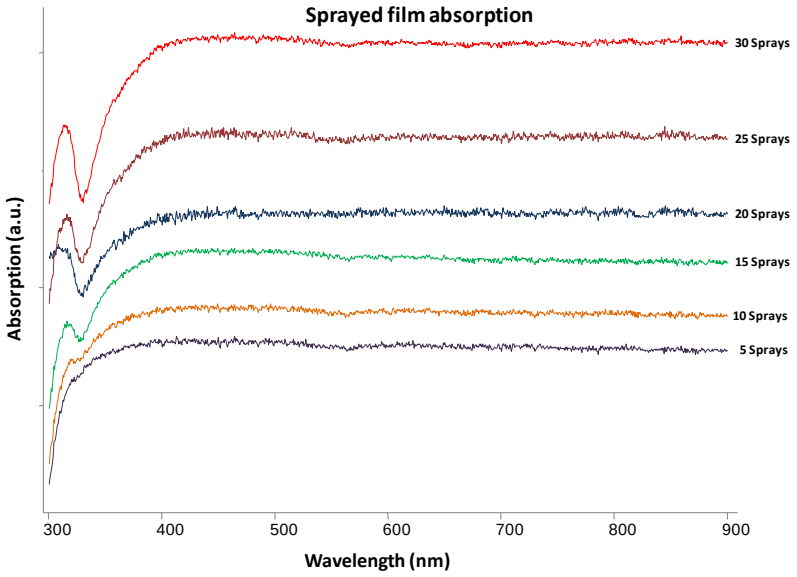

Figure 6.6 Absorption spectrum of the sprayed film.

6.4.3 SEM of Spray Samples.

The SEM images were taken at different magnifications; all samples SEM images were performed in one session. Images were taken with zoomed in focus setting to give a perspective on the distribution of particles among all samples, and then images were taken zoomed out progressively to illustrate the particle distribution in bigger areas of the sample. Keeping in mind that the HFW (horizontal field width) is the measurement across the image and it is displayed in um, also the in the fluorescence measurements, the laser focusing and collective objective used is 20X which gives a probing diameter of 5um.

Figures 6.7-6.10 show the SHIN particles distribution in the spray samples. We see that at 5 sprays while the distribution of the SHIN is even and everywhere, yet there are many areas of the sample that do not have coverage.

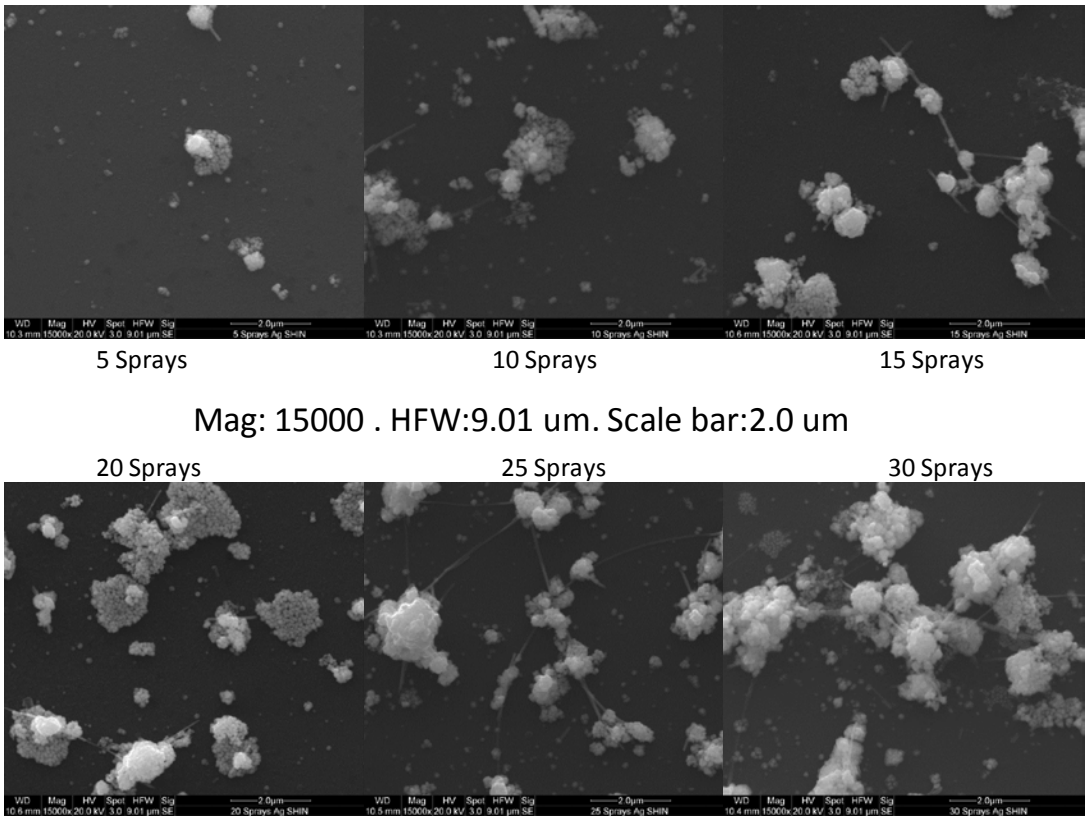

Figure 6.7 SEM images of all SHIN spray samples with 2 µm scale bar.

Images above were taken with the same magnification to illustrate the abundance and distribution of SHIN particles, as the number of SHIN spray increases.

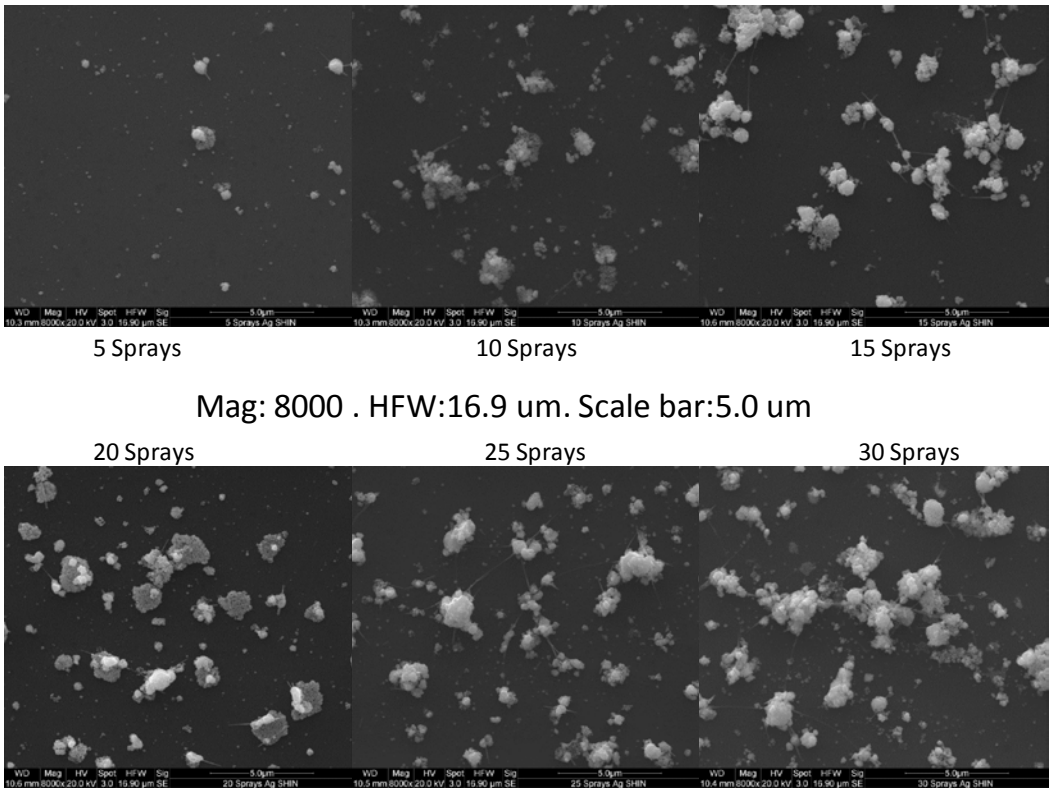

Figure 6.8 SEM images of spray samples with 5 µm scale bar.

As the number of sprays increases, so does the coverage to reach its maximum in 30 sprays. The scale bar in figure 6.8 is 5um which is equivalent to the probing diameter of objective used in fluorescence measurements, we can see that in 5 sprays samples the probability of hitting a spot with a big population of SHIN is significantly lower than other samples, and also the probability is proportional to the number of sprays.

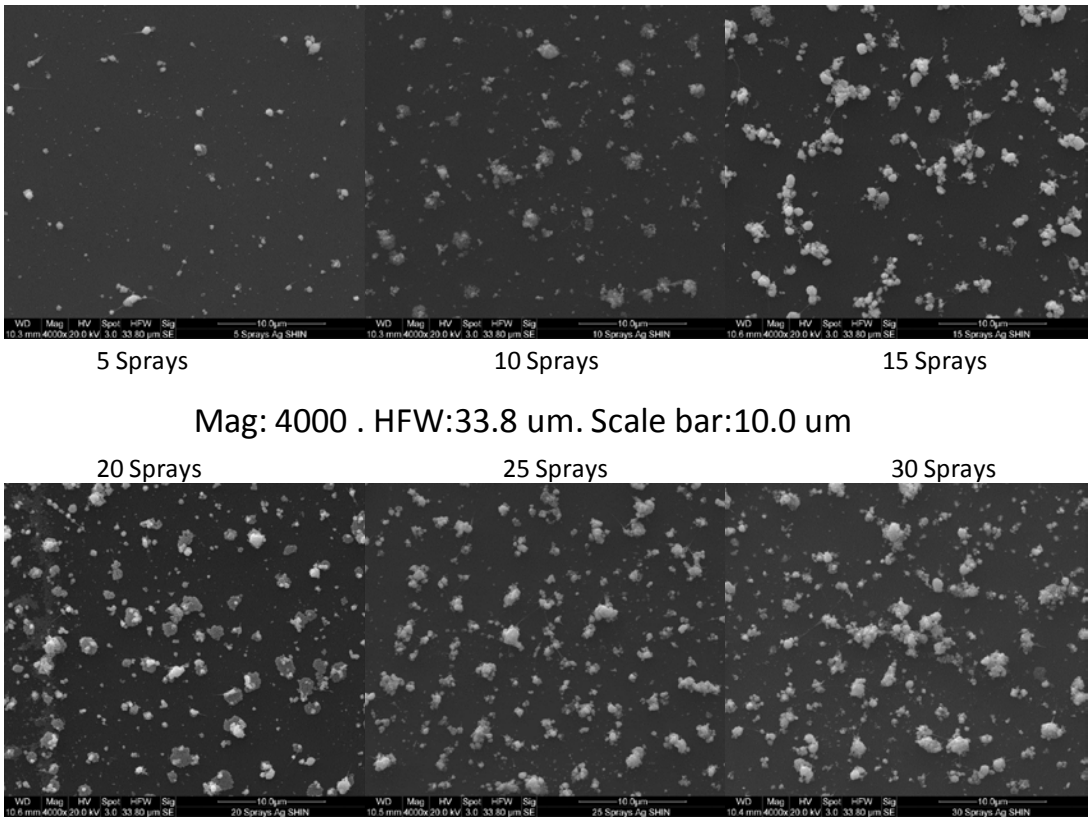

Figure 6.9 SEM images of all SHIN spray samples with 10 µm scale bar.

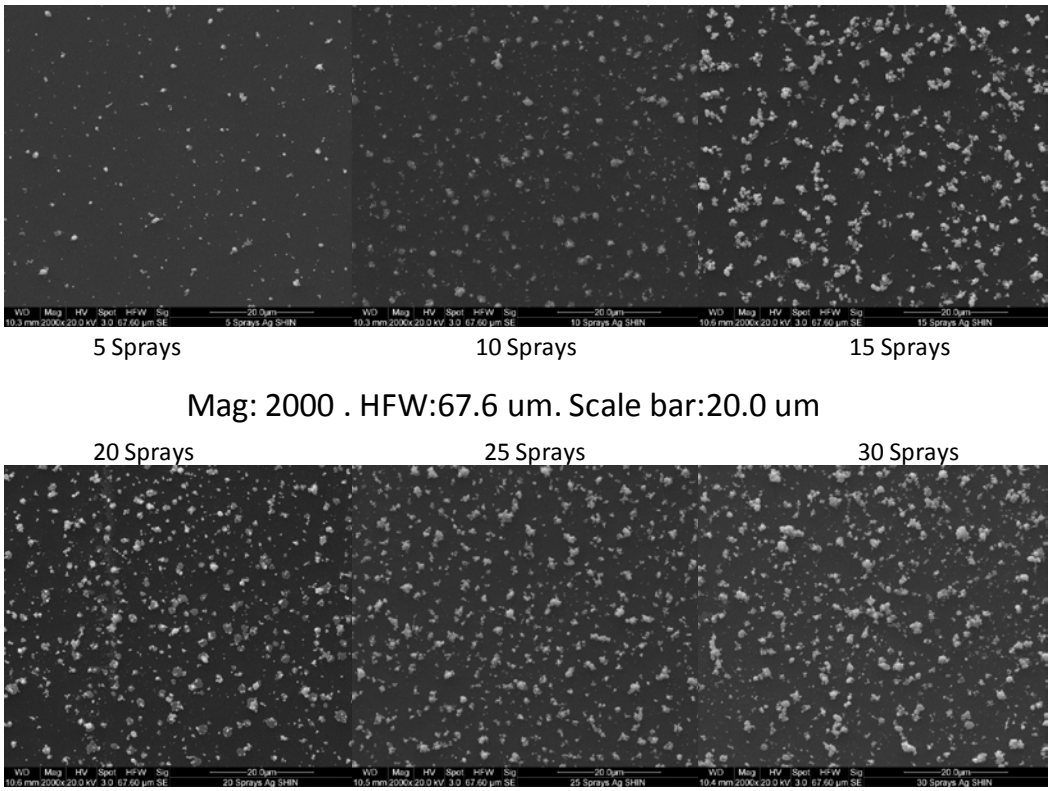

Figure 6.10 An overview of the SHIN spray samples.

6.4.4 EF Histogram of Spray Samples

Fluorescence enhancement factor calculations are done by taking the ratio of SHINEF peak area to the LB reference area. The enhancement factors are tabulated into a histogram distribution showing the right limit of EF value in the x axis with the frequency of occurrence in the y axis. The histograms are shown in figure 6.11(a-g)

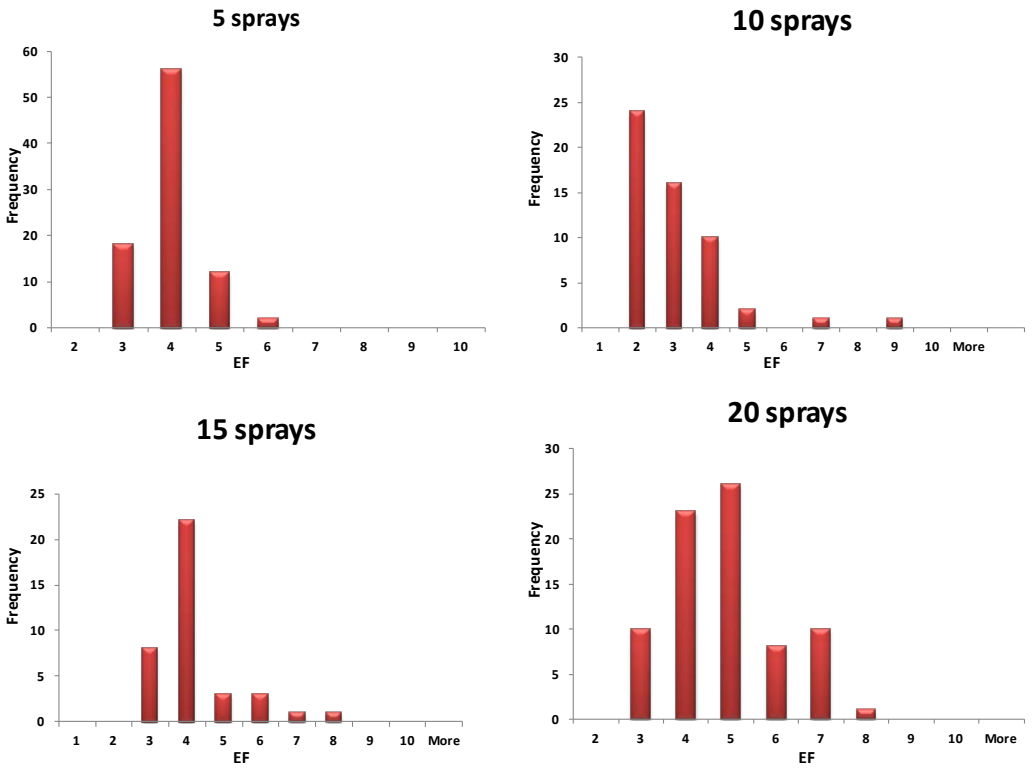

Figure 6.11 (a-d) Enhancement factor (EF) histogram for the spray samples (5, 10, 15, and 20).

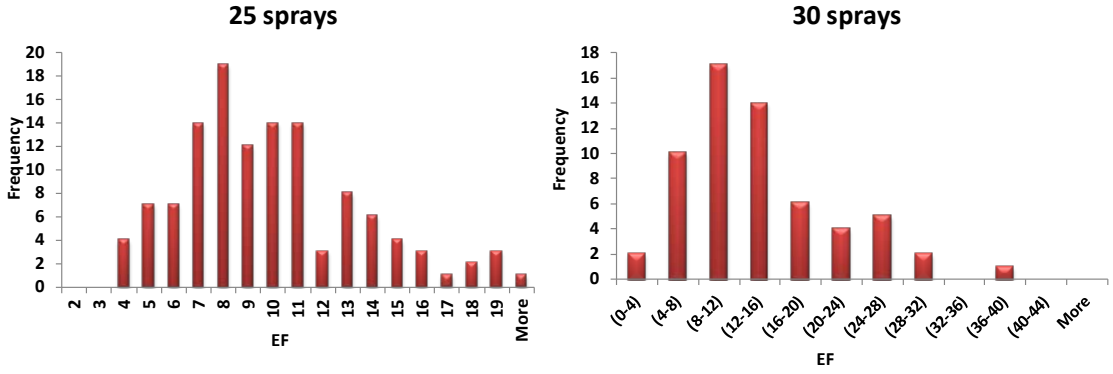

Figure 6.11 (e, f) The histogram of EF for 25, and 30 spray samples.

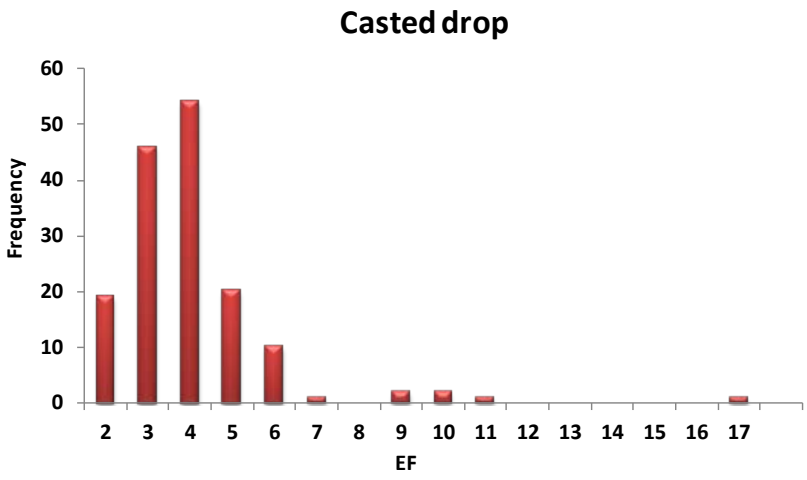

Figure 6.11 (g) EF distribution for a casted drop.

Again we see in the first few samples the maximum enhancement factor increases as the number of sprays increases. The distribution of the enhancement factor shifts toward higher values with increasing shin, especially in the 25 and 30 sprays samples. Enhancement factors as high as 38 could be reached, while highest enhancement factor achieved in casted drop was around 17 for this batch of shin particles. This is not to say that enhancement factors higher than this value are not achievable, what the spray shin samples clearly shows is that with increasing number of sprays, spots with plasmon coupling become more probable due to more homogenous covering of the sample with small aggregates.

6.5 Conclusion

SHIN application by spraying analyte samples provides an increase in efficiency of creating hot spots due to plasmon coupling. Formation of small aggregates group

throughout the analyte surface could be achieved and further tuned with even finer mist spray, to further increase the homogeneity of SHIN aggregates, and the average enhancement factor.

6.6 References

1. Constantino, C.J.L., et al., *Single-molecule detection using surface-enhanced resonance Raman scattering and Langmuir-Blodgett monolayers.* Anal. Chem., 2001. **73**(Copyright (C) 2012 American Chemical Society (ACS). All Rights Reserved.): p. 3674-3678.
2. Kneipp, K., et al., *Single molecule detection using surface-enhanced Raman scattering (SERS).* Phys. Rev. Lett., 1997. **78**(Copyright (C) 2012 American Chemical Society (ACS). All Rights Reserved.): p. 1667-1670.
3. Moula, G. and R.F. Aroca, *Plasmon-Enhanced Resonance Raman Scattering and Fluorescence in Langmuir-Blodgett Monolayers.* Anal. Chem. (Washington, DC, U. S.), 2011. **83**(Copyright (C) 2012 American Chemical Society (ACS). All Rights Reserved.): p. 284-288.
4. Nie, S. and S.R. Emory, *Probing single molecules and single nanoparticles by surface-enhanced Raman scattering.* Science (Washington, D. C.), 1997. **275**(Copyright (C) 2012 American Chemical Society (ACS). All Rights Reserved.): p. 1102-1106.

5. Xu, H.X., et al., *Spectroscopy of single hemoglobin molecules by surface enhanced Raman scattering.* Physical Review Letters, 1999. **83**(21): p. 4357-4360.

6. Kinkhabwala, A., et al., *Large single-molecule fluorescence enhancements produced by a bowtie nanoantenna.* Nature Photonics, 2009. **3**(11): p. 654-657.

7. Zhang, W., et al., *Giant and uniform fluorescence enhancement over large areas using plasmonic nanodots in 3D resonant cavity nanoantenna by nanoimprinting.* Nanotechnology, 2012. **23**(Copyright (C) 2012 American Chemical Society (ACS). All Rights Reserved.): p. 225301/1-225301/9.

8. Guerrero, A.R., Y. Zhang, and R.F. Aroca, *Experimental Confirmation of Local Field Enhancement Determining Far-Field Measurements with Shell-Isolated Silver Nanoparticles.* Small, 2012. **8**(Copyright (C) 2012 American Chemical Society (ACS). All Rights Reserved.): p. 2964-2967.

9. Li, J.F., et al., *Shell-isolated nanoparticle-enhanced Raman spectroscopy.* Nature, 2010. **464**(7287): p. 392-395.

CHAPTER 7

CONCLUSIONS

7.1 Conclusions

In this thesis we have studied, experimentally, the plasmon enhanced fluorescence of high and low quantum yield molecules. The plasmon enhancing nanostructures used in our experiments are shell-isolate nanoparticles; a core of an enhancing metal nanostructure with a nanometric dielectric coating of SiO_2.

In chapter 2, the basic concepts of fluorescence phenomena and properties of localized surface plasmon resonances are discussed. The theory predicts that the basic mechanisms for optically enhanced fluorescence would be in the absorption enhancement, in the modification of the radiative and non-radiative decay rates, and the enhancement via the nanoparticle scattering of the molecular emission.

In chapter 3 we discussed the chemical methods used to synthesize the nanoparticles, the techniques used for LB fabrication and surface characterization, as well as the spectroscopic measurements.

In chapter 4, we confirmed the role of plasmon in enhancing the fluorescence of bis(3,4-dichlorobenzylimido) perylene (chloro-PTCD) molecules fabricated in a mixed LB monolayer. The PTCD series are unique in the fact that when they aggregate, they exhibit an excimer emission that is in a different spectral region relative to the monomer emission. When we used spherical Au-SHINs with scattering matching the emission wavelength of the monomer, we noticed a preferential enhancement to the monomer. When Au-SHIN rods with plasmon bandwidth overlapping with the excimer emission are used, an enhancement of the excimer emission is favored. This shows the plasmon scattering to be a powerful source of contribution to the enhancement, which leads to the

enhanced fluorescence spectra in both Au-SHIN cases to be greatly different from the reference LB fluorescence.

In chapter 5, we study PEF for different dyes with contrasting intrinsic quantum yield values. We use a series of dyes with low quantum yield values, namely crystal violet and ethyl violet with Au-SHINs and Ag-SHINs. The dyes' emission contains both Raman scattering and fluorescence emission. It is found that both processes benefitted equally from the presence of coated nanoparticles. The local field (E_{loc}) extracted from SHINEF enhancement experiments correlates with square value of the local electric field $|E|^2$, while the value extracted from SHINERS show a $|E|^4$ dependence, independent of the intrinsic quantum yield.

The results obtained with malachite green are particularly unique. The electric field enhancement found from SHINEF and SHINERS are similar only when the emission with the plasmon scattering is in the same spectral region.

However, the E_{loc} relationship for SHINEF and SHINERS is reinstated again in malachite green, when the exciting laser is moved closer to the molecular emission, and the plasmon bandwidth is overlapping with fluorescence. Finally a direct comparison between the enhanced emission of two fluorophores with differing quantum yield values, R18 and chromeo 642 is presented. SHINEF enhancement factor are found be comparable for the two dyes using Ag-SHIN, an indirect indication that all fluorophores should benefit equally from the plasmon enhancement provided there is an overlap between the fluorophore emission and the SHIN scattering dipole. The results are for an average

plasmon enhancement of fluorescence. Plasmon enhancement of fluorescence at hot spots is outside the scope of the present work.

In chapter 6, we tested a simple, inexpensive, and practical method of depositing SHIN particles, without the need for surface preparation. As the spraying rounds are increased, there is an increase in the average enhancement factor value compared to the values obtained by drop casting. The method proved effective as the spray droplets covered the surface with small clusters of SHIN particles, thus hosting multiple sites of plasmon coupling with increasing the average enhancement values.

7.2 Future Work

The SHINs demonstrate to be an important step forward in the analytical enhanced spectroscopy. The work presented here is for an average SHINEF enhancement. To improve the boost, there is a need for the fabrication of SHIN substrates with controllable aggregation. In addition, there is an open challenge in the plasmon enhanced fluorescence at hotspots. The giant local electric field seems to provide enhancement factors that cannot be explained with the theoretical model presented for the average fluorescent enhancement.

VITA AUCTORIS

NAME:	Haider Mohan
PLACE OF BIRTH:	Baghdad, Iraq
YEAR OF BIRTH:	1982
EDUCATION:	Al-Kindy Secondary School, Baghdad, Iraq
	1997-2000
	University of Windsor, Windsor, Ontario
	2004-2010